



RESEARCH

Characteristics of crack growth in brittle solids with the effects of material heterogeneity and multi-crack interaction

Luyu Wang · Zhen-Yu Yin · Weizhong Chen

Received: 18 July 2023 / Accepted: 1 February 2024 / Published online: 27 March 2024
© The Author(s) 2024

Abstract Despite the extensive research on crack propagation in brittle solids, numerous unexplored problems still necessitate in-depth study. In this work, we focus on numerical modeling of multi-crack growth, aiming to explore the effect of material heterogeneity and multi-crack interaction on this process. To do this, an improved singular-finite element method (singular-FEM) is proposed with incorporation of heterogeneity and crack interaction. An efficient algorithm is proposed for simulating multi-crack propagation and interaction. Stress singularity near crack tip is reproduced by the singular elements. The singular-FEM is convenient and cost-effective, as the zone far away from crack tips is directly discretized using linear elements, in contrast to the quadratic or transition elements uti-

lized in traditional FEM. Next, the proposed method is validated through benchmark study. Numerical results demonstrate that the superiority of the singular-FEM, which combines the merits of low cost and high accuracy. Then, the mechanics of crack growth are explored in more complex scenarios, accounting for the effects of crack interaction, loading condition and heterogeneity on crack trajectory, stress field and energy release rate. The findings reveal that the combined effect of heterogeneity and crack interaction plays a critical role in the phenomenon of crack growth, and the proposed method is capable of effectively modeling the process.

Keywords Fracture mechanics · Crack interaction · Stress intensity factor · Material heterogeneity

The animation of crack growth is packaged in the attachment as the supplementary data.

Supplementary Information The online version contains supplementary material available at <https://doi.org/10.1007/s10704-024-00771-w>.

L. Wang · Z.-Y. Yin (✉)
Department of Civil and Environmental Engineering, The Hong Kong Polytechnic University, Hung Hom, Kowloon, Hong Kong SAR, China
e-mail: luyu.wang@polyu.edu.hk

Z.-Y. Yin
e-mail: zhenyu.yin@polyu.edu.hk

W. Chen
Institute of Rock and Soil Mechanics, Chinese Academy of Sciences, Wuhan 430071, China
e-mail: wzchen@whrsm.ac.cn

1 Introduction

The prediction of multi-crack growth in brittle materials is considerably more complex than that in single-cracked materials, primarily due to the interactions between adjacent cracks (de Borst 2022; Zhang et al. 2022). Moreover, the level of complexity will be even more severe in heterogeneous media (Schöller et al. 2022; Wang et al. 2022c). Accurately evaluating the stress field in the vicinity of crack tips is important to the safety design that prevents failure of engineering structures (Al-Ostaz and Jasiuk 1997; Wang et al. 2020; Tan et al. 2021). The accurate prediction of crack trajectory can offer a valuable reference for estimating the life

span of a structure. Therefore, developing an efficient and reliable approach for analysing multi-crack growth in heterogeneous materials is of paramount importance.

Early studies for investigating the crack tip stress field were given by Griffith (1921) and Irwin (1957). They recognised that the failure and rupture of a brittle material are induced by the stress concentration around the crack tips, wherein the surface free energy of crack plays an important role in this process. Irwin (1957, 1968) extended the concept of stress concentration and creatively proposed the singular theory around the crack tip. It is now widely acknowledged as the K -field theory, where the stress intensity factors (SIFs) are denoted by K . After that, numerous studies have been conducted on crack analysis, building upon the SIFs concept inherited from Irwin's theory (Erdogan and Sih 1963; Sih 1991; Wang et al. 2019). However, these works mainly focus on theoretical or semi-analytic analysis, limiting their scope to handling only single cracks or regular multi-crack.

The finite element method (FEM), as a powerful numerical method, was employed for solving problems in fracture mechanics. (Weißgraeber et al. 2016; Sedmak 2018; de Borst 2022). Early pioneering studies were pioneered by Chan et al. (1970) and Mowbray (1970). Chan et al. (1970) pointed out that grid refinement could improve the accuracy of calculating SIFs. In their study, the linear triangle elements were used to discretize the crack tip zone. Similarly, Mowbray (1970) proposed an approach known as the energy release rate method for SIF calculation, eliminating the need for grid refinement. Nevertheless, these studies can not recover the characteristic of stress fail to fully capture the crack tip. To this end, Tracey (1970) devised a novel element, the so-called tip singular element, to reproduce the tip singularity. While this advancement enhances the accuracy of SIFs calculation, it is inconvenient to integrate such element into an existing FEM code. Later, the works of Barsoum (1976) and Henshell and Shaw (1975) laid the groundwork for modern computational fracture mechanics. They proposed an alternative approach which is able to recover the tip stress singularity as done by Tracey (1970). The proposed element was devised based on the concept of isoparametric finite elements. Consequently, they proved that the singular element is a special form of its isoparametric element and can be obtained via collapsing nodes into one tip node. Although a lot of successes have been made by the above works, they merely focus on

stationary cracks and do not consider the propagation of cracks.

To model cracks growth, researchers have made significant contributions to the computational fracture mechanics community. Some representative milestones based on the continuum mechanics include the extended-FEM (XFEM) (Budyn et al. 2004), the adaptive-FEM (Mohmadsalehi and Soghrati 2022), the finite-discrete element method (FDEM) (Wang et al. 2021), the boundary element method (BEM) (Zhang et al. 2019), the material point method (MPM) (Kakouris and Triantafyllou 2017), etc. The numerical methods mentioned above have their own pros and cons. For example, the XFEM possesses the merit of mesh independent but will get in trouble with modeling crack interaction and multi-crack (Weißgraeber et al. 2016; Sedmak 2018; de Borst 2022). Furthermore, the XFEM requires the enrichment on the FEM nodes in the scope of a pre-defined distance to the crack tip, resulting in the increase of degree of freedom (Budyn et al. 2004). The adaptive FEM-based methods use the remeshing technique to track the crack paths, wherein an additional cost should be spent on remeshing to update crack configurations. This procedure is quite expensive and complicated if multi-crack are involved (Alzabdeh et al. 1998; Azadi and Khoei 2011; Dang-Trung et al. 2020), and extra efforts need to be paid for mapping the variables from the old mesh to the new mesh (Nguyen-Xuan et al. 2013). The FDEM uses the cohesive zone model to simulate the failure of materials (Wang et al. 2021). However, an expensive computational cost should be spent to predict the condition of each cohesive element. In addition, the cracks can only propagate along the edges of elements. The BEM has an advantage of relative low computational cost compared to the FEM-based methods (Zhang et al. 2019), but it is prone to trouble when complicated geometries are involved. Although the MPM has been successfully used to model crack growth, it will encounter an issue with multi-crack growth (Kakouris and Triantafyllou 2017; de Borst 2022). In contrast to the methods rooted in the classical continuum mechanics and mesh-dependent methods, in recent years some novel numerical methods have been proposed, such as phase-field (PF) model (Miehe et al. 2010) based on an extended variational principle and peridynamics (Silling et al. 2010) based on the non-local theory. Although these methods have been applied to analyse

material failure, the fundamental theory of them is still being developed.

Despite being vital important, developing a numerical method capable of simulating multi-crack remains unexplored to a large extend. In particular, previous studies on crack tip elements mainly focused on modifying the quadratic triangular elements to the quarter-point elements (Henshell and Shaw 1975; Barsoum 1976; Dang-Trung et al. 2020). However, this treatment leads to the elements that are far away from the crack tips being quadratic as well, resulting in an expensive cost. Alternatively, one can simply use the linear triangular element over the global computational domain (Chan et al. 1970; Mowbray 1970), but the numerical accuracy is problematic, since it can not recover the stress singularity. Moreover, those methods will encounter some complicated procedures when simulating crack growth, such as the adaptive meshes and remeshing technique. To this end, this study proposes an improved singular-FEM. It allows to integrate the effect of material heterogeneity and straightforwardly model the multi-crack growth and their interaction. The stress singularity in the vicinity of crack tips can be recovered by the five-node singular triangular elements. The zone far away from the tips can be directly treated by the linear triangular elements instead of the quadratic or transition elements in the traditional FEM. This method is rooted in the rigorous SIFs-based Griffith-Irwin crack theory, which is different from the smeared crack models and the damage mechanics-based methods (e.g. the PF method (Miehe et al. 2010) and the cohesive zone elements (Wang et al. 2021; Romanowicz 2022)).

The paper is organised as follows: a fracture mechanics model for multi-crack analysis is provided in Sect. 2; the singular-FEM is then formulated, and the calculation method of SIFs and crack propagation algorithm are elaborated in Sect. 3; next, numerical validation on benchmarks is performed in Sect. 4; some insights to the mechanism of effects of crack interaction and heterogeneity on crack growth are explored based on simulations.

2 Formulation of multi-crack growth

2.1 Fracture mechanics model

The presented model is formulated within the framework of linear elastic fracture mechanics (Sih 1991;

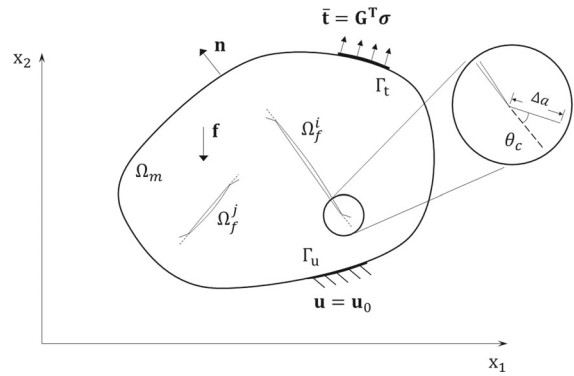


Fig. 1 Fracture mechanics model with multi-crack growth

Zehnder 2012). In this study, we consider a situation of multi-crack growth. As displayed in Fig. 1, the matrix component of the deformable medium Ω is denoted as Ω_m . There are N_f cracks distributed inside the domain, denoted as $\Omega_f = \sum_{i=1}^{N_f} \Omega_f^i$. Consequently, the deformable medium is composed of $\Omega = \Omega_m \cup \Omega_f$.

Consider a linear quasi-statics 2D elastic problem, the deformable medium satisfies the equilibrium equation (Zienkiewicz and Taylor 2000; Bathe 2006). The matrix form is written as:

$$\mathbf{L}^T \boldsymbol{\sigma} = -\mathbf{b} \tag{1}$$

where $\boldsymbol{\sigma}$ is the stress tensor in Voigt notation, \mathbf{b} is the body force. The operator \mathbf{L} is defined as:

$$\mathbf{L} = \begin{bmatrix} \frac{\partial}{\partial x_1} & 0 \\ 0 & \frac{\partial}{\partial x_2} \\ \frac{\partial}{\partial x_2} & \frac{\partial}{\partial x_1} \end{bmatrix} \tag{2}$$

The matrix form of stress tensor reads:

$$\boldsymbol{\sigma} = \mathbf{C}\boldsymbol{\varepsilon} = \mathbf{C}\mathbf{L}\mathbf{u} \tag{3}$$

where \mathbf{C} is the elasticity matrix, $\boldsymbol{\varepsilon}$ is the strain tensor, \mathbf{u} is the displacement vector. As shown in Fig. 1, the boundary conditions are defined on the external boundaries Γ_t and Γ_u :

$$\begin{aligned} \mathbf{u} &= \mathbf{u}_0 \quad \text{on } \Gamma_u \\ \mathbf{G}^T \boldsymbol{\sigma} &= \bar{\mathbf{t}} \quad \text{on } \Gamma_t \end{aligned} \tag{4}$$

where \mathbf{u}_0 and $\bar{\mathbf{t}}$ are the prescribed displacement and traction, respectively. The matrix \mathbf{G} is composed by the outward unit vector $\mathbf{n} = [n_1 \ n_2]^T$, given by:

$$\mathbf{G} = \begin{bmatrix} n_1 & 0 \\ 0 & n_2 \\ n_2 & n_1 \end{bmatrix} \tag{5}$$

Assuming the crack i , denoted as Ω_f^i , will propagate with an increment Δa due to the external loadings, the crack growth direction θ_c is determined by the stress state around the crack tip. Fracture mechanics theory captures the singularity of stress at crack tip by the stress intensity factors (SIFs) K_I and K_{II} (Kanninen et al. 1986; Zehnder 2012). As illustrated in Fig. 2, in the polar coordinate system (r, θ) , the circumferential stress σ_θ and tangential stress $\sigma_{r\theta}$ around the tip of a mixed-mode crack are expressed as (Kanninen et al. 1986; Zehnder 2012):

$$\begin{aligned}\sigma_\theta(r, \theta) &= \frac{1}{\sqrt{2\pi r}} \cos \frac{\theta}{2} \left(K_I \cos^2 \frac{\theta}{2} - \frac{3}{2} K_{II} \sin \theta \right) \\ &= \frac{K_I^{eq}}{\sqrt{2\pi r}} \\ \sigma_{r\theta}(r, \theta) &= \frac{1}{2\sqrt{2\pi r}} \cos \frac{\theta}{2} [K_I \sin \theta + K_{II} (3 \cos \theta - 1)] \\ &= \frac{K_{II}^{eq}}{\sqrt{2\pi r}}\end{aligned}\quad (6)$$

where K^{eq} is the equivalent SIF for a mixed-mode crack (Erdogan and Sih 1963; Sih 1991). It can be calculated by the SIFs (K_I and K_{II}) of pure mode-I and II cracks. The details of numerical implementation will be discussed in Sect. 3.

2.2 Multi-crack growth

The maximum circumferential stress (MCS) criterion (Erdogan and Sih 1963; Sih 1991) is employed to determine crack propagation condition and crack growth direction θ_c . As depicted in Fig. 2, θ_c needs to be evaluated at each step based on the current stress state.

(1) Crack growth direction. The stress state around crack tip at Step n is given in Eq. (6). Therefore, the direction θ_c is obtained by solving $\partial\sigma_\theta/\partial\theta = 0$ and $\partial^2\sigma_\theta/\partial\theta^2 < 0$ according to MCS criterion:

$$\theta_c = 2 \arctan \left(\frac{K_I \pm \sqrt{K_I^2 + 8K_{II}^2}}{4K_{II}} \right) \quad (7)$$

(2) Propagation criterion. The critical value of the equivalent SIF K_I^{eq} in Eq. (6) is obtained by substituting θ_c . It can be re-written as:

$$K_I^{eq} = \cos \frac{\theta_c}{2} \left(K_I \cos^2 \frac{\theta_c}{2} - \frac{3}{2} K_{II} \sin \theta_c \right) \quad (8)$$

The crack branch shown in Fig. 2 will emerge once the circumferential stress equals to the critical stress. It

can be evaluated by the fracture toughness K_{IC} :

$$\sqrt{2\pi r} \sigma_\theta(r, \theta_c) = K_I^{eq} \geq K_{IC} \quad (9)$$

(3) Crack increment. Assume each of the cracks has different increments at each computation step, Δa^i for crack i is determined by Paris-type law (Kanninen et al. 1986; Zehnder 2012):

$$\Delta a^i = \Delta a_{max}^i \left(\frac{G_f^i}{G_{max}} \right)^\alpha \quad (10)$$

where Δa_{max}^i is the maximum increment during crack propagation. It equals to the initial length L_f^i of crack as suggested in literature (Paluszny and Matthäi 2009). The numerical parameter α equals to 0.35 as suggested in literature (Renshaw and Pollard 1994; Dang-Trung et al. 2020). G_{max} is the maximum energy release rate among all of the cracks in the domain. The energy release rate G_f^i for crack i is formulated as:

$$G_f^i = \frac{(1+\nu)(1+k)}{4E} \left[(K_I^{eq})^2 + (K_{II}^{eq})^2 \right] \quad (11)$$

where the equivalent SIFs are defined in Eq. (6). E and ν are Young's modulus and Poisson's ratio, respectively. $k = (3 - \nu)/(1 + \nu)$ for plane stress problem and $k = 3 - 4\nu$ for plane strain problem.

As depicted in Fig. 2, the deflection and propagation increment of a crack depend on the stress state around crack tip, in which stress singularity at the tip is evaluated by the SIFs. The details of calculating SIFs will be elaborated in Sect. 3.

3 Numerical approach

3.1 Formulation of Galerkin FE framework

The improved singular triangular elements are integrated into the Galerkin FE framework to capture the characteristics of stress singularity (Liu et al. 2010; Nguyen-Xuan et al. 2013). This integration constitutes the singular-FE method, which is formulated based on the weak form of the governing equation Eq. (1):

$$\int_{\Omega} \mathbf{u}^T \mathbf{L}^T \mathbf{C} \mathbf{L} \mathbf{v} d\Omega - \int_{\Gamma_t} \mathbf{G}^T \boldsymbol{\sigma} \mathbf{v} d\Gamma - \int_{\Omega} \mathbf{b} \mathbf{v} d\Omega = 0 \quad (12)$$

where \mathbf{v} is the test function in finite element method. The aim of solving Eq. (12) is to find $\mathbf{u} \in V_S$ with $\forall \mathbf{v} \in V_T$. The test space V_T and solution space V_S satisfy the

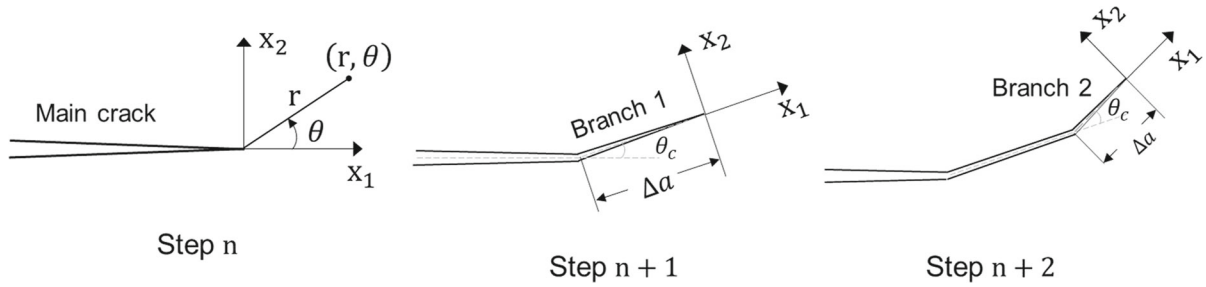


Fig. 2 Schematic of crack growth at different stages

following conditions (Zienkiewicz and Taylor 2000; Dang-Trung et al. 2020):

$$\begin{aligned}
 V_T &= \left\{ \mathbf{v} \in H^1(\Omega), \mathbf{v}|_{\Gamma_u} = 0 \right\} \text{ and} \\
 V_S &= \left\{ \mathbf{v} \in H^1(\Omega), \mathbf{v}|_{\Gamma_u} = \mathbf{u}_0 \right\}
 \end{aligned}
 \tag{13}$$

where $H^1(\Omega)$ is the Sobolev space of functions. Displacement \mathbf{u} is approximated by the Galerkin finite element method:

$$\mathbf{u} \approx \mathbf{u}_h = \sum_{i=1}^{n_{node}} \mathbf{N}_i \mathbf{U}_i = \mathbf{N} \mathbf{U}
 \tag{14}$$

where \mathbf{U} is the displacement vector located at grid vertices. n_{node} is the number of nodes in the finite element grids. \mathbf{N} is the shape function matrix containing all nodes. For node i , the matrix reads:

$$\mathbf{N}_i = \begin{bmatrix} N_i(\mathbf{x}) & 0 \\ 0 & N_i(\mathbf{x}) \end{bmatrix}
 \tag{15}$$

where $N_i(\mathbf{x})$ is the shape function of node i .

Then, the weak form Eq. (12) can be further written as the fully discretized form:

$$\mathbf{K} \mathbf{U} = \mathbf{F}
 \tag{16}$$

The global stiffness matrix \mathbf{K} and external force matrix \mathbf{F} are formulated as:

$$\begin{aligned}
 \mathbf{K} &= \int_{\Omega} \mathbf{N}^T \mathbf{L}^T \mathbf{C} \mathbf{L} \mathbf{N} d\Omega \text{ and} \\
 \mathbf{F} &= \int_{\Omega} \mathbf{N}^T \mathbf{b} d\Omega + \int_{\Gamma_f} \mathbf{N}^T \mathbf{G}^T \boldsymbol{\sigma} d\Gamma
 \end{aligned}
 \tag{17}$$

The linear triangular elements (LTEs) are used to discretize the regions that are not directly connected to the crack tip. Especially, the LTEs offer the advantage of low computational cost since it is sufficient for regions far away from tips. The convenience stems from the fact that the shape functions can be formulated in

the same manner as in the standard FEM (Liu et al. 2010; Nguyen-Xuan et al. 2013):

$$\begin{bmatrix} N_1^L(\mathbf{x}) \\ N_2^L(\mathbf{x}) \\ N_3^L(\mathbf{x}) \end{bmatrix} = \frac{1}{2\Delta A} \begin{bmatrix} y_{23} & x_{32} & x_2 y_3 - x_3 y_2 \\ y_{31} & x_{13} & x_3 y_1 - x_1 y_3 \\ y_{12} & x_{21} & x_1 y_2 - x_2 y_1 \end{bmatrix} \begin{bmatrix} x \\ y \\ 1 \end{bmatrix}
 \tag{18}$$

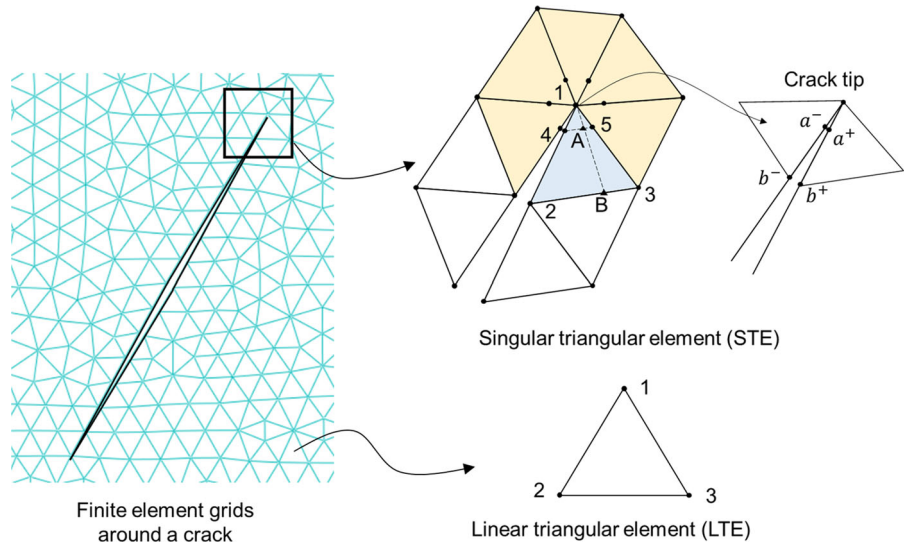
where $x_{ij} = x_i - x_j$ and $y_{ij} = y_i - y_j$ for $i \neq j$ and $(i, j = 1, 2, 3)$. The area of element is calculated by $\Delta A = (x_{32}y_{12} - x_{12}y_{32})/2$.

3.2 An improved singular-FEM

It is worth mentioning that the shape function matrix \mathbf{N}_i has different forms for the finite elements in the vicinity of a crack tip compared to those far away from the tip. The reason is that the stress distribution at the crack tip often exhibits the $1/\sqrt{r}$ stress singularity, as indicated by the stress field (Eq. (6)). This characteristic necessitates that the elements around the crack tip can effectively reproduce the singularity.

In the displacement-based finite element method, the stress singularity requires a displacement field with the term \sqrt{r} because stress is the derivative of displacement. Herein we follow the formulation of an adaptive singular FEM proposed in literature (Liu et al. 2010; Nguyen-Xuan et al. 2013). The five-node singular triangular elements (STEs) are assigned around the crack tips to describe the singular stress field with arbitrary order, as shown in Fig. 3. Note that the improved singular elements differ from the traditional quarter-point elements (Henshell and Shaw 1975; Barsoum 1976; Dang-Trung et al. 2020), which are typically required even in regions far away from the tips to ensure compatibility, while such limitation is addressed in the proposed framework.

Fig. 3 Finite element grids around a crack and the schematics of STE and LTE



The displacement of an arbitrary point $P(x, y)$ within a crack tip element can be expressed by the interpolation of displacements of node 1 (the crack tip node), point A and point B. The displacement component u reads (Liu et al. 2010; Nguyen-Xuan et al. 2013):

$$u = c_1 + c_2r + c_3\sqrt{r} \tag{19}$$

where c_i ($i = 1, 2, 3$) are the coefficients determined by the displacement components of node 1, point A and point B, denoted by u_1, u_A and u_B .

In Fig. 3, point A is positioned on the line connecting the singular nodes 4 and 5, whereas point B is positioned on the line connecting nodes 2 and 3. The accurate locations can be determined through interpolating with the coordinates of nodes 2 ~ 5 (Liu et al. 2010). The definition of r is illustrated in Fig 2. It measures the radial distance from the crack tip in a polar coordinate system. Substituting u_1, u_A and u_B into Eq. (19), one can obtain the expanded formula:

$$u = \phi_1u_1 + \phi_2u_A + \phi_3u_B \tag{20}$$

where the interpolation function ϕ_i ($i = 1, 2, 3$) are expressed by:

$$\begin{bmatrix} \phi_1 \\ \phi_2 \\ \phi_3 \end{bmatrix} = \begin{bmatrix} 1 & 2 & -3 \\ 0 & -4 & 4 \\ 0 & 2 & -1 \end{bmatrix} \begin{bmatrix} 1 \\ r/l_{B-1} \\ \sqrt{r/l_{B-1}} \end{bmatrix} \tag{21}$$

where l_{B-1} is the length of edge B-1, as illustrated in Fig. 3.

Displacement u_1 in Eq. (20) is a node-based quantity which is the primary unknown in the singular-EFM. However, as shown in Fig. 3, u_A and u_B are not the

node-based quantities and should be expressed by the interpolation of displacements of nodes 2, 3, 4 and 5 of this element:

$$\begin{aligned} u_A &= (1 - \eta)u_4 + \eta u_5 \\ u_B &= (1 - \eta)u_2 + \eta u_3 \end{aligned} \tag{22}$$

where η is the distance fraction and defined by $\eta = l_{A-4}/l_{5-4} = l_{B-2}/l_{3-2}$ (Liu et al. 2010; Nguyen-Xuan et al. 2013).

Substituting Eqs. (21) and (22) into Eq. (20), the general form of displacement components u within a STE can be written as:

$$u = \sum_{i=1}^5 N_i^S(\mathbf{x})u_i \tag{23}$$

where $N_i^S(\mathbf{x})$ ($i = 1, \dots, 5$) are the shape functions of five nodes of STE. The subscript S represents the five-node singular triangular elements. They are formulated as:

$$\begin{aligned} N_1^S &= \phi_1, \quad N_3^S = \eta\phi_3, \quad N_5^S = \eta\phi_2 \\ N_2^S &= (1 - \eta)\phi_3, \quad N_4^S = (1 - \eta)\phi_2 \end{aligned} \tag{24}$$

3.3 Calculation of stress intensity factors (SIFs)

As discussed in Sect. 2.2, the evolution of cracks highly depends on the evaluation of SIFs K_I and K_{II} . There are many methods developed for calculating SIFs, typically the interaction integral method (Liu et al. 2010), the energy domain integral method (Moran and

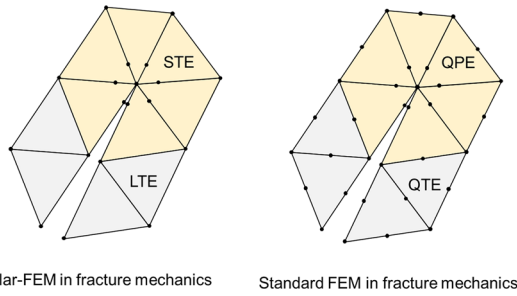


Fig. 4 Different types of finite elements used in fracture mechanics (STE: the improved singular triangular element; LTE: linear triangular element; QPE: quarter-point element; QTE: quadratic triangular element)

Shih 1987), and the displacement extrapolation method (Kuang and Chen 1993).

The methods based on integral are often used in the analysis of single-crack problem. However, if the multi-crack are involved, the calculation of integrals in the vicinity of each of the crack tips is quite complicated. Here we do not intend to compare different computation methods. In this study, we utilize the displacement extrapolation method (Kuang and Chen 1993), which has been extensively applied in computational fracture mechanics (Guinea et al. 2000; Dang-Trung et al. 2020).

The SIFs can be expressed by the nodal displacements of singular elements and material properties (Kuang and Chen 1993; Guinea et al. 2000):

$$K_I = \frac{E}{6(1 + \nu)(1 + k)} \sqrt{\frac{2\pi}{h_{tip}}} (8\Delta U_{ay} - \Delta U_{by})$$

$$K_{II} = \frac{E}{6(1 + \nu)(1 + k)} \sqrt{\frac{2\pi}{h_{tip}}} (8\Delta U_{ax} - \Delta U_{bx})$$

(25)

where h_{tip} is the average size of crack tip elements around the crack tip. The capital letter U indicates that it is a node-based quantity (primary unknown). As depicted in Fig. 3, the tangential components of relative displacements between the node pairs $a^+ - a^-$ and $b^+ - b^-$ are ΔU_{ax} and ΔU_{bx} . Similarly, the normal components are ΔU_{ay} and ΔU_{by} .

It is worth mentioning that the displacement extrapolation method has been successfully applied in the standard FEM for fracture mechanics simulation. However, one of the drawbacks of standard FEM is that the quadratic triangular elements (QTEs) should be utilized even in regions far away from the crack tips to guarantee displacement compatibility (Henshell and Shaw

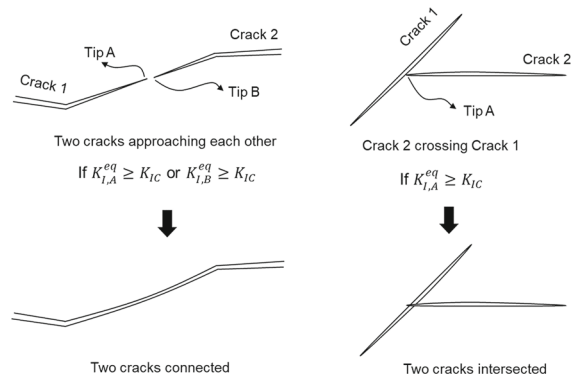


Fig. 5 Schematic of two interacting cracks approaching or crossing each other

1975; Barsoum 1976), as displayed in Fig. 4. It leads to some unnecessary computational costs. In contrast, this limitation is resolved in the proposed singular-FEM.

3.4 Algorithm for crack propagation and interaction

The state of crack propagation is highly dependent on the stress conditions around crack tips. In numerical implementation, the SIFs of each crack tip need to be evaluated. Actually, the calculation of SIFs based on displacement extrapolation (Eq. (25)) is stress-independent and only the node-based displacements are involved, wherein the displacement vector is calculated by the FE formulation Eq. (16). The solution strategy is summarized in the following steps:

- (1) Generate the multi-crack in the computational domain and define the coordinates of each crack tip.
- (2) Discretize the computational domain using Delaunay triangulation. The grid resolution depends on the minimum size of cracks (Shewchuk 2002; Wang et al. 2022a, c).
- (3) At each step, calculate SIFs according to Eq. (25) for all crack tips; calculate the equivalent SIF using Eq. (8), then determine whether the crack grows or not based on Eq. (9).
- (4) If the crack satisfies propagation criterion, crack growth direction and crack increment are determined by Eqs. (7) and (10), respectively.
- (5) Update crack tip coordinates for all propagated cracks. The grids are correspondingly updated using Delaunay triangulation for computation in the next step.

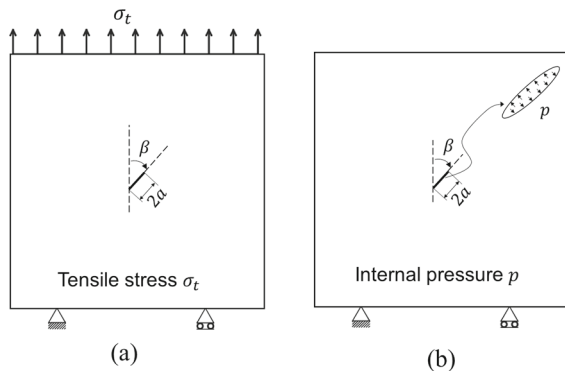


Fig. 6 Schematics of a plate with a crack under **a** tensile loading and **b** internal pressure

Modeling of interaction between two cracks that are approaching or crossing each other has attracted widespread attention. A previous study proposed a strategy to simulate interacting cracks by the adaptive-FEM (Paluszny and Matthäi 2009). However, as they claimed in the literature, this method can easily result in an issue of grid distortion and will encounter some unexpected troubles in mesh adaptive procedure. Therefore, we introduce an efficient method to alleviate the troublesome grid operations, as displayed in Fig. 5. We directly use the SIF-based MCS criterion Eq. (9) to predict growth of such interacting cracks, where $K_{I,A}^{eq}$ and $K_{II,B}^{eq}$ are the equivalent SIFs of crack tips A and B. In Sect. 4, we will show that the improved singular-FEM is able to simulate multi-crack growth and their interaction.

4 Results and discussion

In this section, the improved singular-FEM is used to analyse the stress field and crack propagation in the deformable media under different configurations. After a series of numerical tests, we are concerned about the influences of multi-crack, crack interaction, loading conditions and material heterogeneity on crack trajectory and crack tip field.

4.1 Model performance: comparison of different methods

First, we consider a plate containing a single crack to validate the numerical method and investigate the stress

field and displacement around the crack tip. The material is a kind of brittle material (plexiglas). The size of the 2D computational domain is $10\text{ cm} \times 10\text{ cm}$. A crack with inclined angle β and length $2a = 1\text{ cm}$ is placed in the center of the domain, as shown in Fig. 6a.

A tensile loading is imposed on the top side of the specimen ($\sigma_t = 1\text{ MPa}$). The bottom side is fixed. In this situation, the equivalent SIF K_I^{eq} is smaller than the fracture toughness K_{IC} such that the crack remains stationary. We analyse the stress field with various inclined angles $\beta = 30, 60$ and 90 degrees. As reported in literature (Erdogan et al. 1962; Yukio et al. 1983), Young's modulus and Poisson's ratio of plexiglas are $4 \times 10^6\text{ psi}$ (equals to 2.76 GPa) and 0.31 , respectively. The fracture toughness K_{IC} of plexiglas is 4.6 kgf/mm^2 (equals to $1.425\text{ MPa} \cdot \sqrt{\text{m}}$) (Yukio et al. 1983). According to Eq. (8), when $K_I^{eq} < K_{IC}$, the equivalent SIF reads:

$$K_I^{eq} = \cos \frac{\theta}{2} \left(K_I \cos^2 \frac{\theta}{2} - \frac{3}{2} K_{II} \sin \theta \right) \quad (26)$$

where both K_I and K_{II} can be calculated either by analytical solution or by numerical methods. For a stationary crack, the analytical SIFs are formulated as $K_I = \sigma_t \sqrt{\pi a} \sin^2 \beta$ and $K_{II} = \sigma_t \sqrt{\pi a} \sin \beta \cos \beta$ (Erdogan and Sih 1963; Sih 1991). In addition, the SIFs can also be computed numerically by Eq. (25).

To evaluate the accuracy of singular-FEM, the numerical solutions of the stress field in the vicinity of the crack tip are compared with the results obtained by the commercial software ABAQUS (Smith 2009). The element type is CPS6 with the collapse of element sides to generate the singular elements in the software. Fig. 7 provides a comparison between the solutions obtained by the improved singular-FEM and ABAQUS. The x -axis is a normalised distance \bar{x} along the crack length. Moreover, it can be seen that both the stress components σ_θ and $\sigma_{r\theta}$ at the crack tip are relatively larger than other positions. The angle β measures the degree of the crack inclination, therefore the crack is a pure mode-I fracture in the case of a horizontal crack. It can also be indicated in Fig. 7 that $\sigma_{r\theta}$ equals to zero when $\beta = 90^\circ$.

To quantitatively measure the accuracy, we compare the difference of K_I^{eq} between the results calculated by the singular-FEM and the analytical solution. The error is defined by:

$$\epsilon_h = \frac{\|\bar{K}_I^{eq} - \tilde{K}_I^{eq}\|_2}{\|\bar{K}_I^{eq}\|_2} \quad (27)$$

Fig. 7 Stress fields of **a** circumferential stress σ_θ and **b** tangential stress $\sigma_{r\theta}$ at the crack tip with various inclined angles

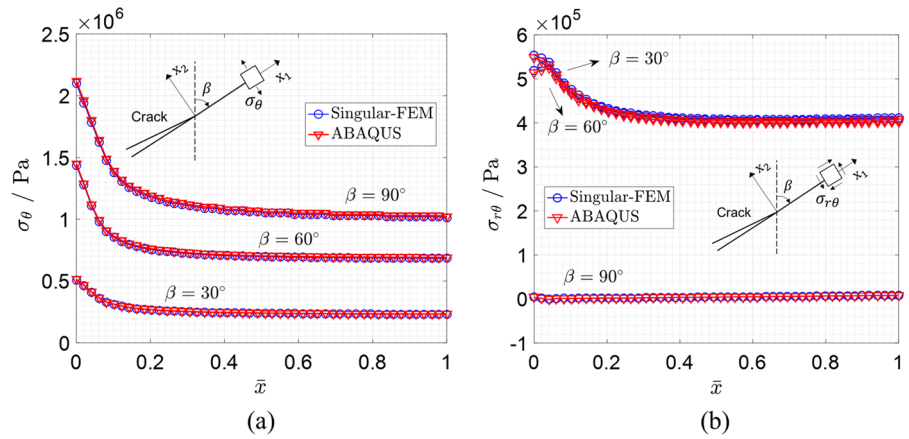


Fig. 8 Grid convergence with different grid resolutions h_{min} . The error ϵ_h is evaluated by the difference of K_I^{eq} calculated by the improved singular-FEM and analytical solution

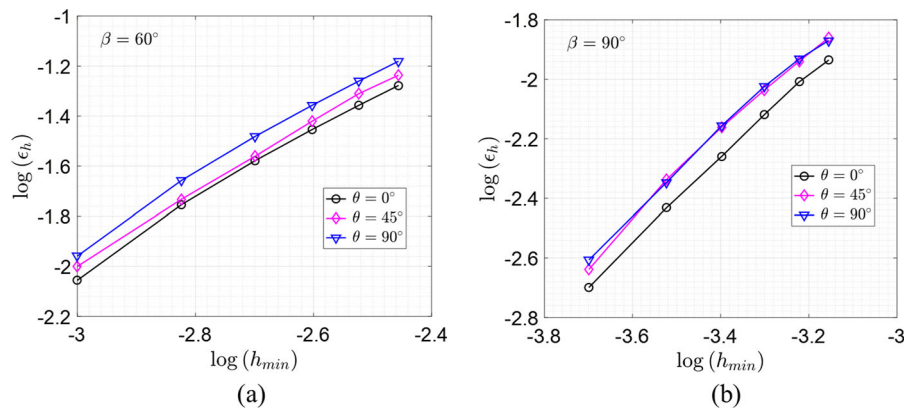
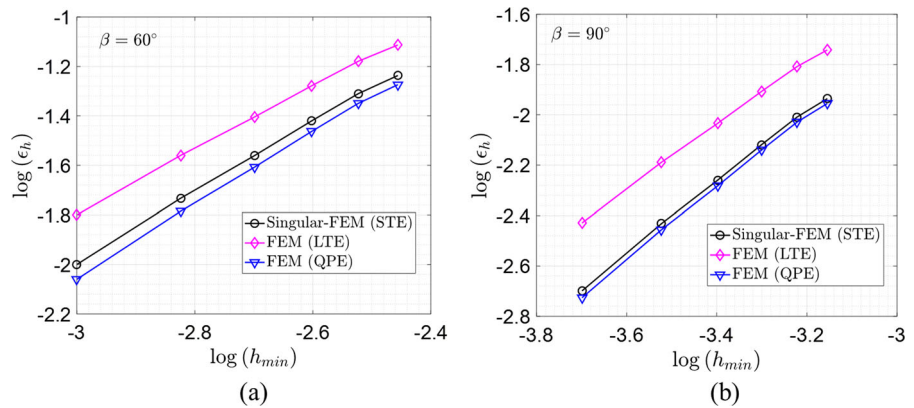


Fig. 9 Comparison of grid convergence with different grid resolutions h_{min} . The error ϵ_h is calculated by different types of the crack tip elements

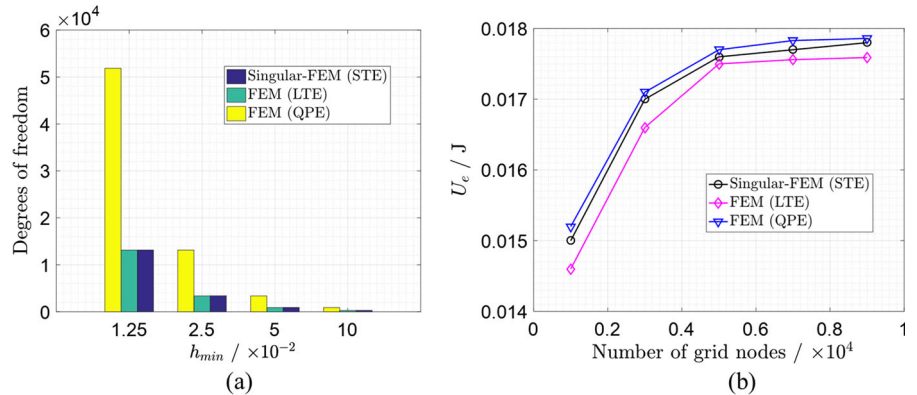


where \bar{K}_I^{eq} and \tilde{K}_I^{eq} are the analytical and numerical values, respectively.

Different inclined angles β have influences on the K_I^{eq} as well as numerical accuracy. In this context, we examine the convergence performance with two angles $\beta = 60^\circ$ and 90° . The error indicator ϵ_h is calculated with different grid resolutions h_{min} , where ϵ_h is the minimum size over all finite elements. As demonstrated

in Figs. 8 and 9, the convergence is almost a linear relation during reducing grid size. A similar result can also be found in our recent publication related to stress analysis of the fractured media (Wang et al. 2022a). Moreover, the convergence results prove that the improved singular-FEM is more accurate than those of FEM with linear triangular element (LTE) and almost as accurate as quarter-point element (QPE).

Fig. 10 Comparison of a degrees of freedom and b convergence of the strain energy with different types of the crack tip elements



The strain energy U_e is calculated to evaluate the convergence performance of different numerical schemes. It is calculated by:

$$U_e = \int_{\Omega} \frac{1}{2} \boldsymbol{\sigma}^T \boldsymbol{\varepsilon} d\Omega \quad (28)$$

As shown in Fig. 10b, the strain energy calculated by different methods approximate to a constant value with the increase of grid refinement. The simulations were executed on an Intel Core i7-7950 processor at 2.6 GHz with 16 GB memory. In a quasi-static problem with 9000 nodes, the CPU times (unit: seconds) for the singular-FEM, LTE and QPE methods are 386, 355 and 591, respectively. Note that in this case the reference solution is 0.0179 J. The simulation results show that the results of FEM (LTE) is smaller than those of singular-FEM and FEM (QPE). Although the FEM (QPE) is slightly more accurate than the singular-FEM, at the cost of higher degrees of freedom, where the expensive cost significantly increase as the computational scale increases, as displayed in Fig. 10a. The improved singular-FEM provides a compromise strategy that combining the merits of low cost and high accuracy.

To further demonstrate the reliability of the presented method, we consider another loading condition, where the internal pressure p is imposed on the crack surface, as shown in Fig. 6b. Model parameters are the same as the above model. We are concerned about the opening δ_f between the two sides of crack. The analytical solution reported in literature (Ucar et al. 2018; Wang et al. 2022a) reads:

$$\delta_f = \frac{2ap(1-\nu)}{G} \sqrt{1 - \left(\frac{\eta}{a}\right)^2} \quad (29)$$

where η is the local coordinate on the crack surface ($0 \leq \eta \leq 2a$). The shear modulus G is related to E via

$E = 2G(1 + \nu)$. We consider a stationary crack where the analytical solution is applicable.

Figure 11 proves that a good matching exists between the analytical and numerical solutions. Crack opening at the middle position of the crack surface reaches the maximum value. A similar study was also given in literature (Ucar et al. 2018; Wang et al. 2022a). In general the curve of crack opening induced by the internal pressure has a parabolic shape for any arbitrary angle β . In addition, the strain energy U_e is calculated to evaluate the convergence performance of the improved singular-FEM with different inclined angles β , as shown in Fig. 11. It demonstrates that in this case U_e is independent of β . The strain energy converges to a certain value with the grid refinement.

4.2 Characteristics of a propagated crack in homogeneous media

To simulate a propagated crack, the external loading σ_t is increased to 10 MPa such that the equivalent SIF $K_I^{eq} > K_{IC}$. The material parameters are the same as the above. The crack length is 2 cm with an inclined angle 45° , and the size of the specimen is 20 cm \times 20 cm, as shown in Fig. 12.

The experimental result of an inclined propagated crack in a brittle plate is reported by Erdogan and Sih (1963). It is observed that the crack propagates along a specific direction, extending in a wing-shaped pattern. Crack growth represents a progression of material deterioration, eventually terminating when the crack reaches the boundaries of the domain. The results indicate that the crack propagates horizontally, aligning with the orientation perpendicular to the maximum stress. Therefore, Fig. 12 illustrates a good matching

Fig. 11 Comparison of numerical results and analytical solution (a) and convergence of the strain energy

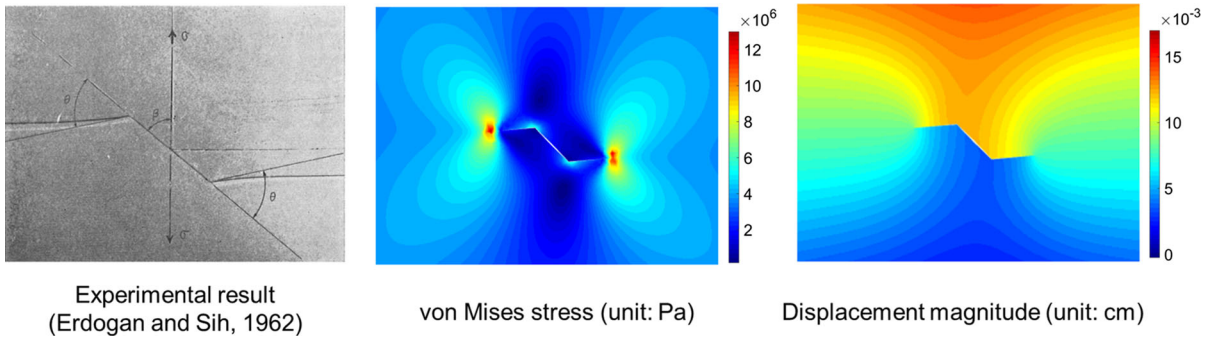
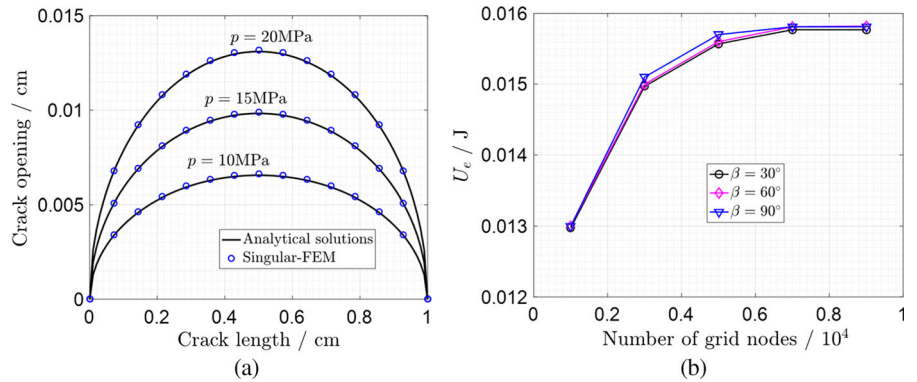


Fig. 12 Comparison of crack trajectory of an inclined propagated crack obtained by experiment and numerical simulation

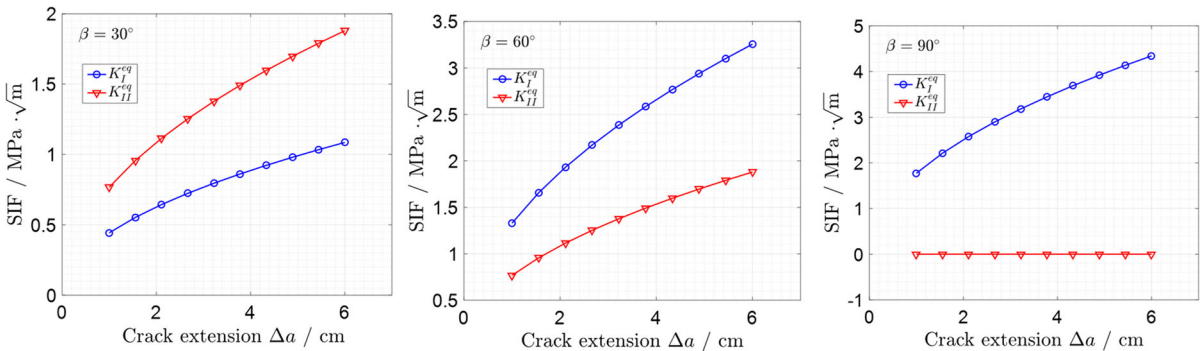


Fig. 13 Variation of the SIFs K_I^{eq} and K_{II}^{eq} with different inclined angles and crack extension

between the experimental result and the numerical solution. We can also reasonably infer that any inclined crack will propagate along the horizontal direction under uniaxial tensile loading.

The dominance of mode-I and II fractures is varied with the inclined angle β , as shown in Fig. 13. Both the SIFs K_I^{eq} and K_{II}^{eq} equal to zero in the case of a vertical crack ($\beta = 0^\circ$), while K_I^{eq} plays a dominant

role when $\beta = 90^\circ$ since in this context there is no shear component existing in the vicinity of the crack tip.

A plate containing an edge crack is displayed in Fig. 14. We are intended to compare the crack trajectories simulated by the presented method with that of the existing results. This problem has been studied in the existing literature (Rao and Rahman 2000; Azó-

Fig. 14 Crack trajectory in an edge cracked plate. The results extracted from [Nguyen-Xuan et al. \(2013\)](#) (top), the vertical displacement (middle) and the shear stress (bottom) calculated by the improved singular-FEM (unit: dimensionless)

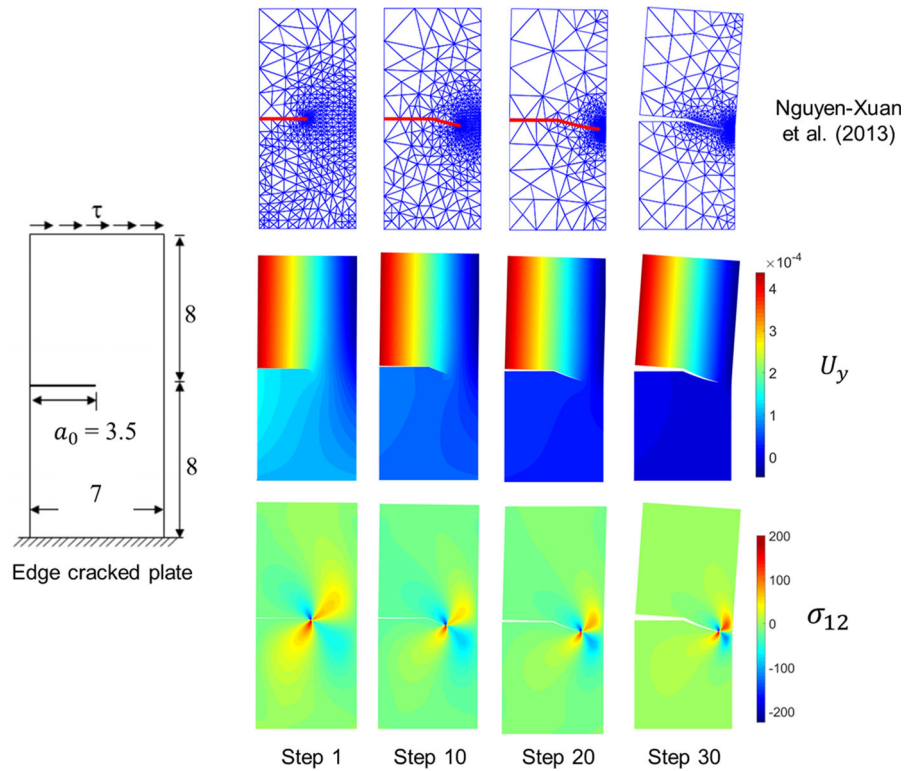
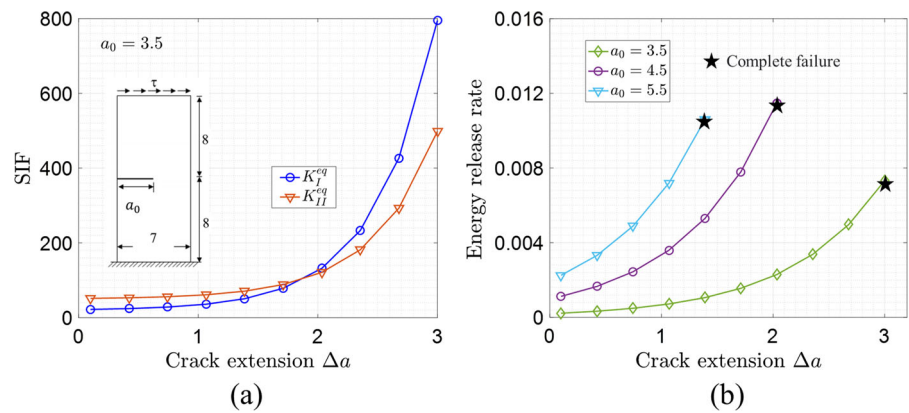


Fig. 15 Variation of **a** SIFs and **b** energy release rate with crack extension (unit: dimensionless)

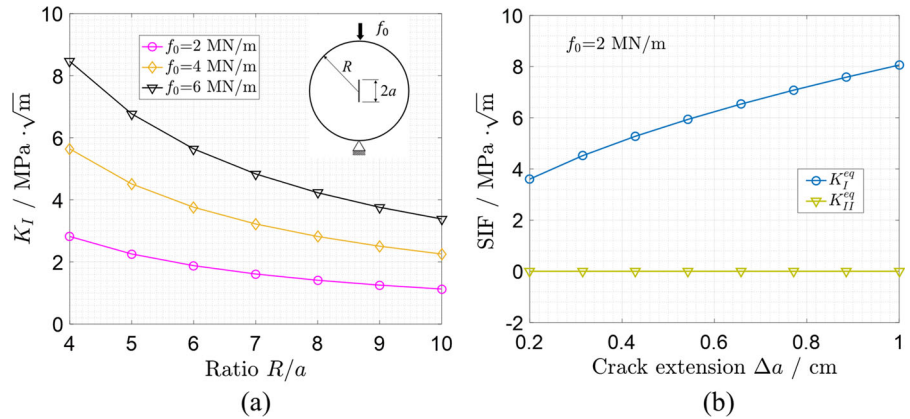


[car et al. 2010](#); [Nguyen-Xuan et al. 2013](#)). We follow the parameters used in the literature ([Rao and Rahman 2000](#)), wherein the variables are dimensionless. The height and width of the model are 16 units and 7 units, respectively. A horizontal edge crack is placed in the middle of the left side. Young’s modulus and Poisson’s ratio are 30×10^6 units and 0.25, respectively. The shear stress τ imposed on the top surface is 1 unit. As displayed in [Fig. 14](#), the crack propagates along an oblique direction rather than the horizontal direction, since the external shear loading induces a different stress field

compared with the uniaxial loading. Obviously, in this context K_{II} plays a dominant role relative to K_I . In addition, we provide the distributions of vertical displacement U_y as well as shear stress σ_{12} , wherein the shape of crack tip zone relies on the propagation steps.

The relation of SIFs and crack extension is displayed in [Fig. 15a](#). The dominance of SIFs depends on the increase of crack extension Δa . For instance, it is observed that K_{II}^{eq} (shear failure) dominates over K_I^{eq} (tensile failure) when $\Delta a \leq 1.9$. The specimen is completely destroyed once the crack propagation reaches

Fig. 16 Brazilian disk model. **a** The size effect and **b** variation of SIFs with crack extension. The unit MN/m equals to MPa · m



the right boundary of the specimen. Figure 15b provides the variation of energy release rate with crack extension. It shows that different values of initial length a_0 of crack have effect on energy release, where the asterisks marked in this figure indicate the energy release rate when the specimen is complete failure. The rate of change of energy release for a large crack is relatively higher compared to that of small cracks. It can be interpreted by a fact that energy release rate is equivalent to the surface energy, which is dependent on the size of the crack.

4.3 Brazilian disk test and effect of heterogeneous material

The Brazilian disk test has been widely investigated in crack analysis and it is a benchmark for validating numerical results (Atkinson et al. 1982; Bouchard et al. 2000; Haeri et al. 2014; Dang-Trung et al. 2020). Especially, for a disk containing a center pre-existing crack, both the experimental and analytical analyses have proven that the crack trajectory is almost a straight line along the vertical direction (Bouchard et al. 2000; Haeri et al. 2014).

As illustrated in the inset in Fig. 16a, a disk model is established to study crack growth. The specimen is a brittle material. Young’s modulus and Poisson’s ratio are 25 GPa and 0.21, respectively. The fracture toughness of the disk specimen is $K_{IC} = 2 \text{ MPa} \cdot \sqrt{\text{m}}$ (Atkinson et al. 1982). The length of the central crack is $2a = 10 \text{ mm}$ and the radius of the disk specimen is $R = 42 \text{ mm}$. The bottom of the computational domain is fixed. The external loading is controlled by a line load f_0 (unit: MN/m) and it is applied on the top of

the disk. In 2D problem, the load is calculated by $f_0 h_t$ and h_t is the thickness of the specimen. The size effect has an influence on the SIF K_I , as depicted in Fig. 16a. The ratio R/a is defined by the disk radius to the half length of the crack. The numerical solution shows that K_I^{eq} is smaller than the fracture toughness K_{IC} when $f_0 = 2 \text{ MN/m}$ and $R/a \geq 7$. It appears that the SIF tends to a stable value if the ratio is greater than 8, since the size effect will disappear if the crack length is small enough compared to the disk size. The SIF K_I^{eq} varies with the increase in crack extension, as shown in Fig. 16b. In addition, K_{II}^{eq} is a constant in this process since the crack is placed along the horizontal direction, therefore the failure mode is purely tensile.

Figure 17 shows the contours and crack trajectory in a homogeneous elastic medium. The distributions of displacement and stress fields (von Mises stress and shear stress) are governed by the condition of crack growth. Obviously, the crack propagates along the vertical direction since the crack is subjected to a tensile stress in the Brazilian test, and the failure is a mode-I fracture (Atkinson et al. 1982). As we expected, the crack path obtained by the improved singular-FEM is in agreement with the experimental results reported in literature (Haeri et al. 2014).

The above numerical simulations are based on a homogeneous medium. However, many studies point to the important of material heterogeneity in mechanical characteristics of fractured media. In particular, crack growth in heterogeneous media differs from crack growth in homogeneous media (Budyn et al. 2004), since the heterogeneity may alter the stress field and affects the crack interaction. To study the influence of heterogeneity, we generate a heterogeneous medium

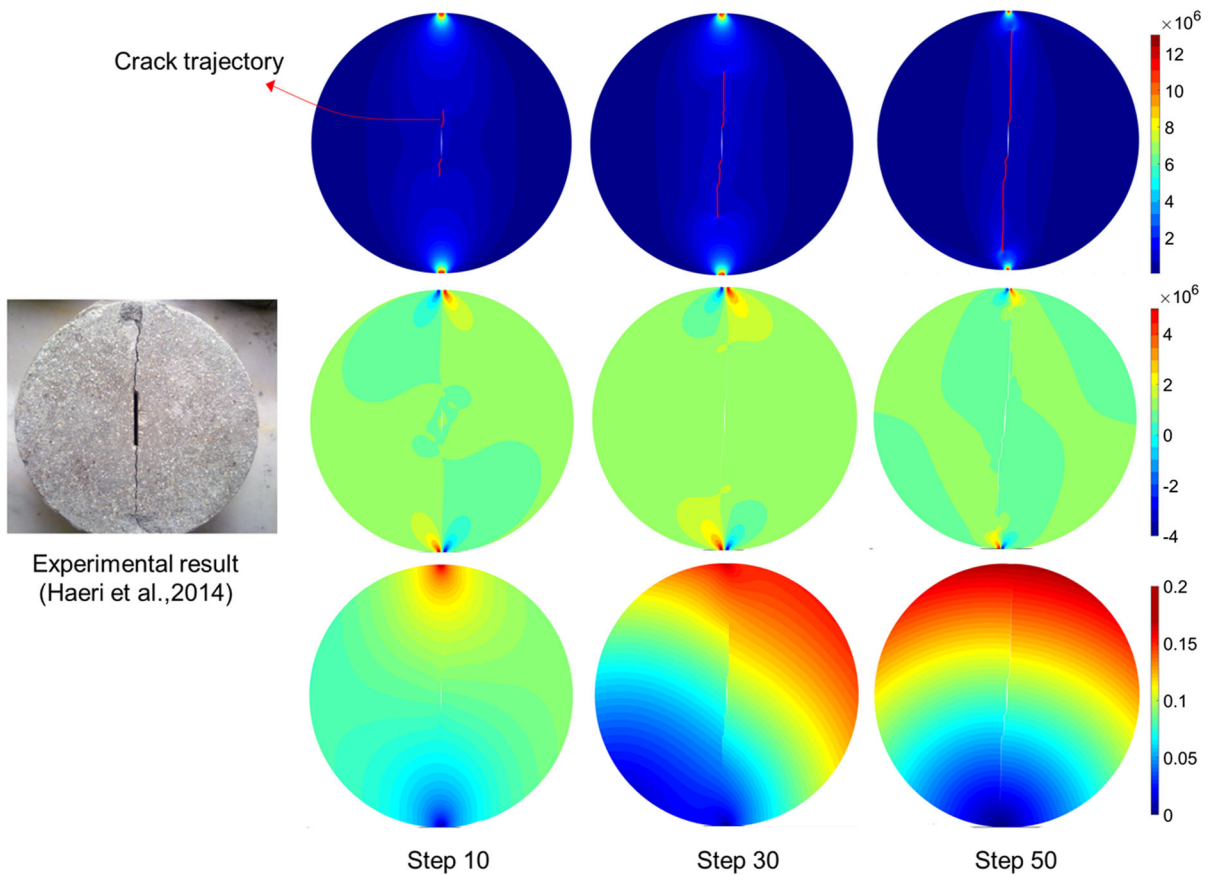


Fig. 17 Crack growth in the Brazilian disk model. The von Mises stress (top, unit: Pa), the shear stress (middle) and the displacement (bottom, unit: cm). The animation of crack growth is accessible in Supplementary Data

with Pattern A and Pattern B, wherein the heterogeneity is controlled by the random field of Young's modulus E , as illustrated in Fig. 18. The method for generating heterogeneity is similar to the method used in literature (Wang et al. 2022b, c). It is observed that the von Mises stress field is not smooth compared to the case of homogeneity (Fig. 17). The crack trajectories in homogeneous and heterogeneous media are shown in Fig. 19. There are deviations of crack trajectory in heterogeneous cases instead of the vertical direction in homogeneous case. The reason is that the crack tip field is related to the distribution of E , wherein it is a uncertain and random field. Figure 20 provides a comparison of distributions of stress and displacement (along the vertical direction of the disk specimen) between the homogeneous and heterogeneous media. It turns out that the curves in the homogeneous case are relatively smoother than those in the heterogeneous cases. The

effect of heterogeneous fluctuation on stress is more pronounced than on displacement. Despite Pattern B employing a heterogeneous field, its overall displacement closely aligns with that of the homogeneous case. We attribute this observation to the heterogeneity in mechanical properties.

Numerical results prove that material heterogeneity has a slight influence on convergence performance of the proposed singular-FEM as well as the strain energy U_e , as shown in Fig. 21a. On the one hand, the strain energy U_e tends to a stable value when the grid resolution is larger than 7000. On the other hand, U_e in the condition of heterogeneous Pattern A (0.0142 J) is smaller than that of in other two conditions (0.0148 and 0.01496 J). It implies that the effect of heterogeneity leads to a highly uneven stress field distributed over each finite element. In this context the degree of uneven field is also reflected by the difference of com-

Fig. 18 Crack trajectory and von Mises stress field in two patterns of the heterogeneous media of Brazilian disk test. The animation of crack growth is accessible in Supplementary Data

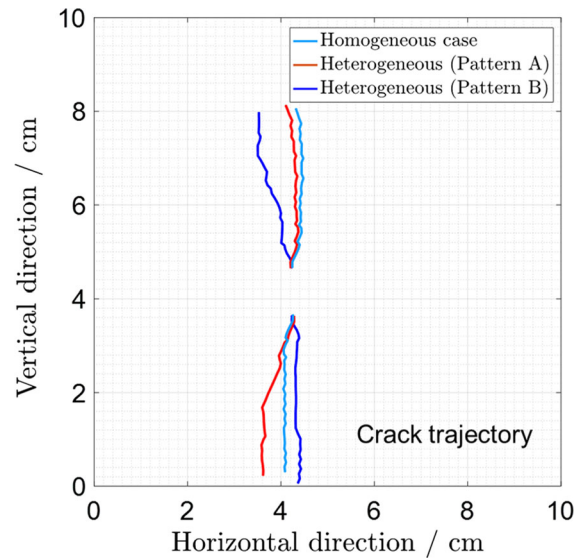
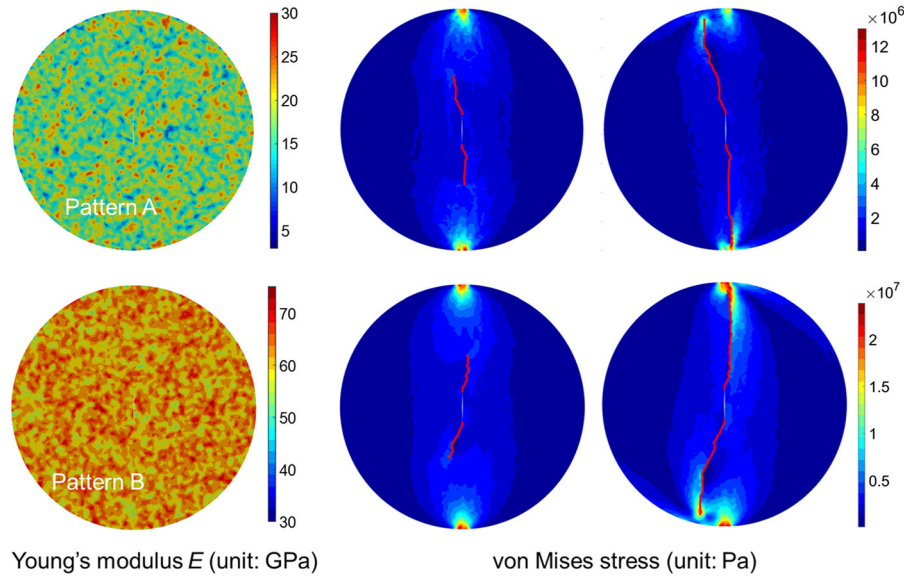


Fig. 19 Comparison of crack trajectories in homogeneous and heterogeneous media of Brazilian disk test

pressive stress-deformation relation obtained from different materials, as displayed in Fig. 21b. Moreover, it appears that the heterogeneity may improve or reduce material strength.

4.4 Propagation of interacting cracks and multi-crack in heterogeneous media

In this section, we analyse crack growth of two interacting cracks as well as multi-crack. First, we focus on

understanding the influence of interaction effects on the crack tip field and crack trajectory. To this end, a plate with two interacting cracks is established, as shown in Fig. 22. The crack on the left side (Crack 1) is placed horizontally and the other one (Crack 2) is inclined with an angle β . The length of both two cracks is $2a = 1$ cm and the angle β is 45° . The size of the computational domain is $10 \text{ cm} \times 10 \text{ cm}$. The external loading applied on the top surface σ_t is controlled by an increased displacement 0.1 mm per step. The specimen is a brittle medium. Young's modulus and Poisson's ratio are 30 GPa and 0.25 , respectively.

The distance H between these two cracks is measured by the line connecting the center points of the cracks. To study the influence of various distance on the degree of interaction, H is set to five values ($H = 1, 2, 3, 4$ and 5 cm) such that the ratio a/H is $1/2, 1/4, 1/6, 1/8$ and $1/10$. The effect of crack interaction is evaluated by the SIFs K_I and K_{II} .

Next, we focus on the tips A and B of Crack 1. The variation of SIFs is shown in Fig. 22. Obviously, the influence of crack interaction on tip A is larger than on tip B, as indicated by the phenomenon that K_I is almost a constant when $a/H \leq 1/4$. The crack interaction can be neglected in the case of $a/H \leq 1/8$ since the distance H is larger enough. However, the degree of interaction is stronger while the tip A is approaching to Crack B, especially when $a/H \geq 1/4$. The result demonstrates that the fracture mode of Crack 1 transitions from pure mode-I to mixed-mode I-II as Crack 1

Fig. 20 Brazilian disk test. Distributions of **a** von Mises stress and **b** displacement when stress state satisfies propagation criterion

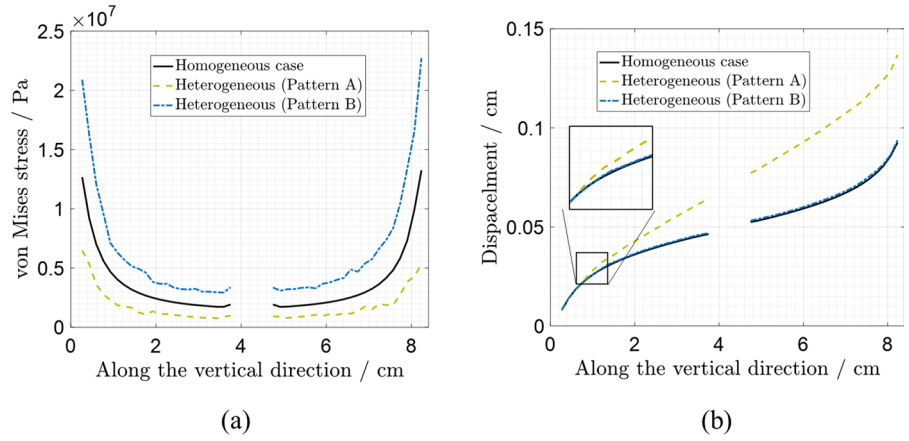


Fig. 21 Brazilian disk test. Convergence of **a** strain energy and **b** influence of material heterogeneity on compressive stress-deformation relation

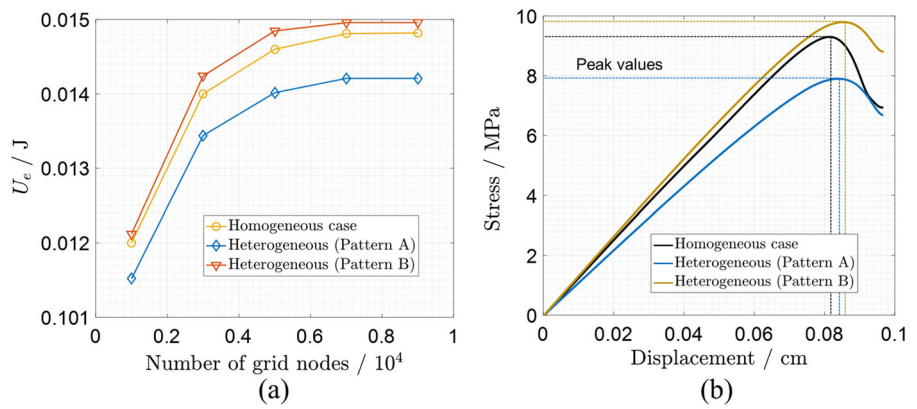


Fig. 22 Influence of the distance between two interacting cracks on the variation of SIFs (K_I and K_{II}) of crack tips A and B

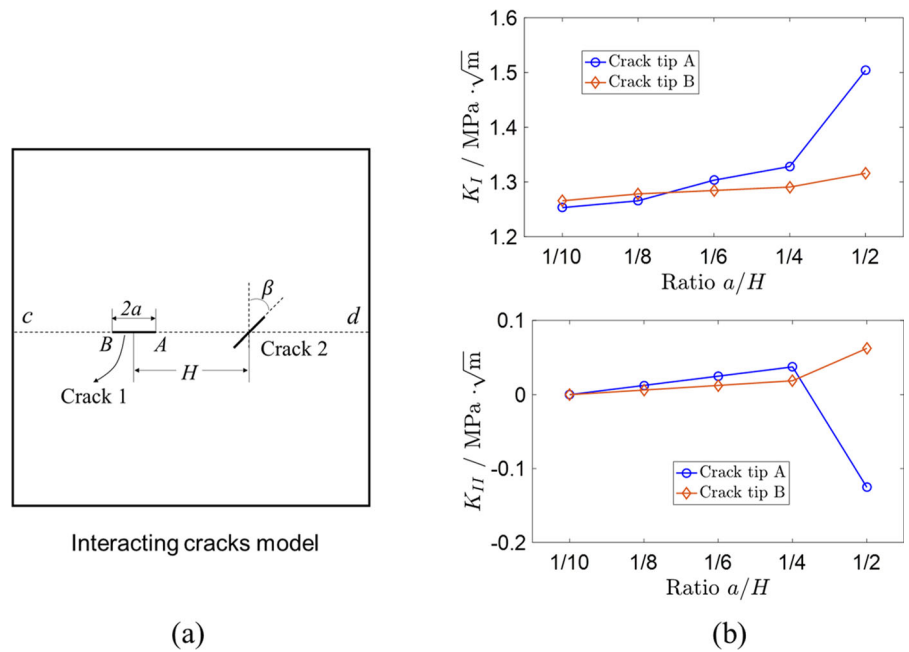
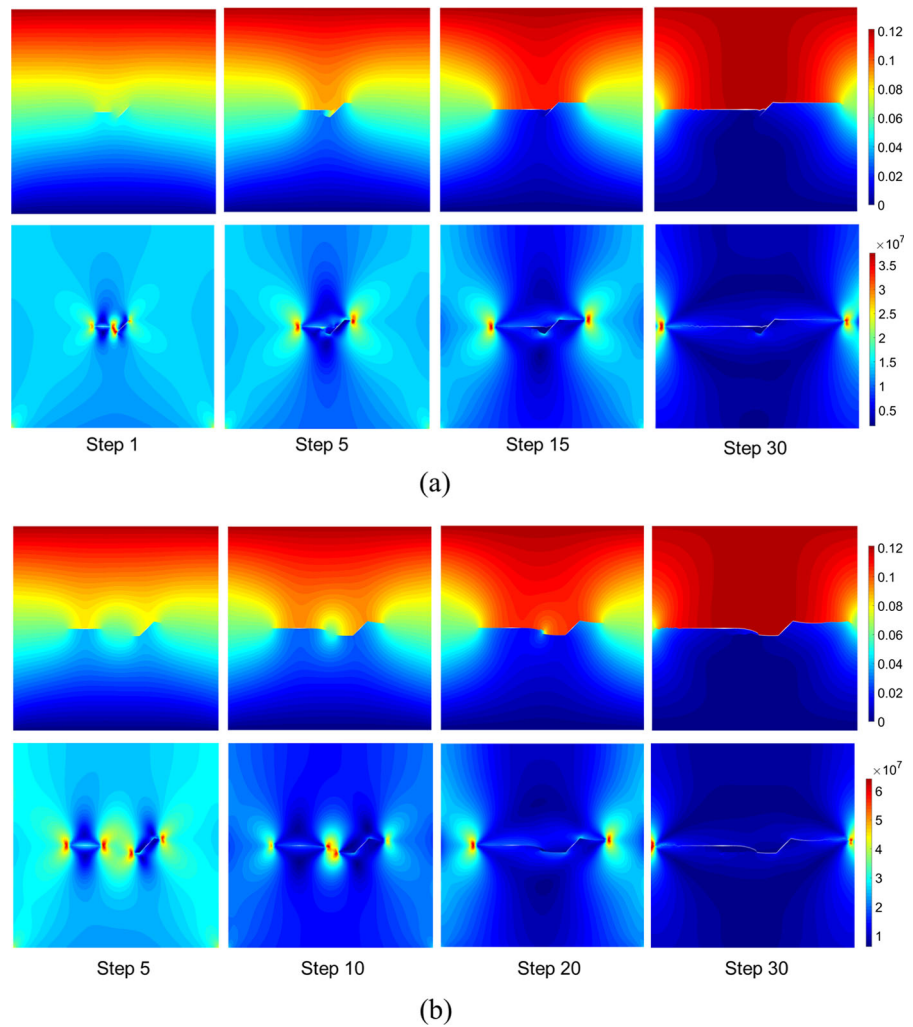


Fig. 23 Crack growth of two interacting cracks with different distances H (a is a fixed value 0.5 cm). In **a** $a/H = 1/2$ and **b** $1/6$, the top and bottom rows are displacement (unit: cm) and von Mises stress (unit: Pa). The animation of crack growth is accessible in Supplementary Data



approaches to Crack 2, accompanied by an increase in the magnitude of SIFs.

Figure 23 shows the displacement field and von Mises stress during crack propagation in the cases of $a/H = 1/2$ and $1/6$. There is a common observation in both the two cases, where Crack 1 and Crack 2 propagate simultaneously, after experiencing the stages of crack growth and crack interaction, then the cracks will eventually coalesce together. The degree of interaction depends on the distance H , as indicated in Fig. 22. It is worth mentioning that the crack trajectories in the interaction zone is not along the horizontal direction when the cracks are almost connected, for instance, Step 15 in Fig. 23a. Figure 24 illustrates a comparison in the cases of $a/H = 1/2$ and $1/6$. It shows the distributions of displacement and stress along a line cd (as displayed

in Fig. 22) across the cracks. The results imply that the effect of crack interaction increases the degree of stress concentration, and the strong discontinuities are caused by the presence of cracks.

A further study demonstrates that the distance between two cracks has strong effect on the variation of energy release rate. The closer the distance, the more energy is released, as illustrated in Fig. 25a. In another aspect, this study further induces that the variation rate of energy release for two cracks very close is larger than that of two distant cracks, as shown in Fig. 25b. The asterisks marked in this figure imply the energy release rate when the two cracks are connected.

A deformable medium with a more complex crack configuration is studied to explore the growth of multi-crack, and to show the presented method is able to sim-

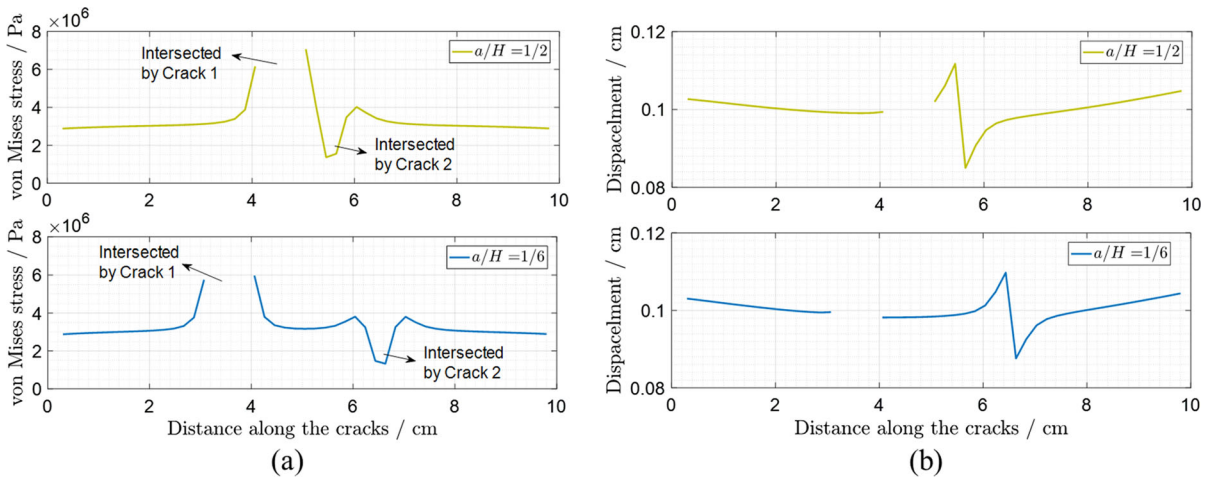
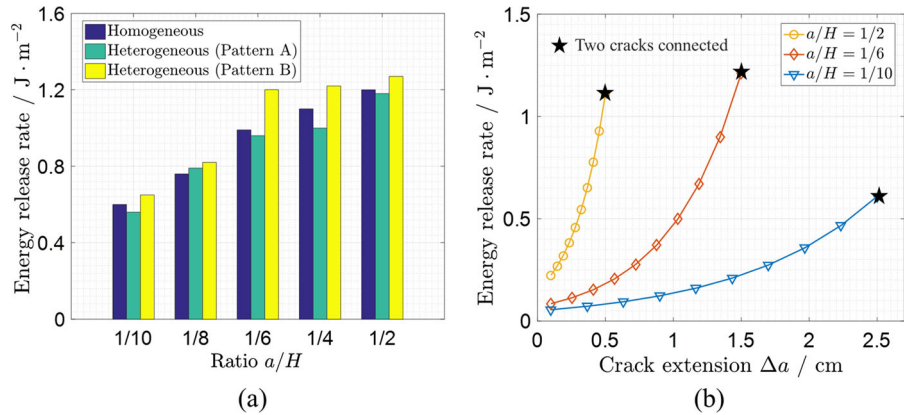


Fig. 24 Distributions of **a** von Mises stress and **b** displacement along line *cd* when stress state satisfies propagation criterion ($a/H = 1/2$ and $1/6$) of the interacting cracks

Fig. 25 Variation of energy release rate with crack extension and in **a** different solid materials in **b** homogeneous material when the two cracks are connected



ulate the interaction of multi-crack. The model parameters are the same above. Ten cracks with length 1 cm are randomly distributed inside the computational domain, as displayed in Fig. 26. First, we consider a homogeneous material. Simulation results imply that the cracks (Cracks 1, 2 and 3) located at the middle of the domain start to grow first because the stress concentration in this zone is significantly higher than other zones. The interaction effect between crack tips leads to the deviation of crack paths. For example, the left tip of Crack 2 tends to approach the right tip of Crack 1. Similarly, the left tip of Crack 3 and the right tip of Crack 2 are tend to coalesce. Eventually, as shown in Step 25 in Fig. 26, these cracks become one major crack, resulting in the fragmentation of the material. Note that the crack trajectory obtained by our method is similar to the results

reported in literature (Budyn et al. 2004; Azadi and Khoei 2011).

It is an interesting theme to study the effect of heterogeneity on crack trajectory, especially for the multi-crack growth. Similar to Sect. 4.3, we generate two different heterogeneous fields (Patterns A and B) controlled by the material property E , as illustrated in Fig. 27. Simulation results show that although the heterogeneity has an effect on crack propagation, the degree of influence depends on the collaboration of random field and crack interaction. The mechanism behind this phenomenon is more complicated than in the case of a single cracked medium, such as the Brazilian disk in Sect. 4.3, since crack interaction plays an important role that cannot be ignored. In summary, whether it is a homogeneous material or a heterogeneous material, in

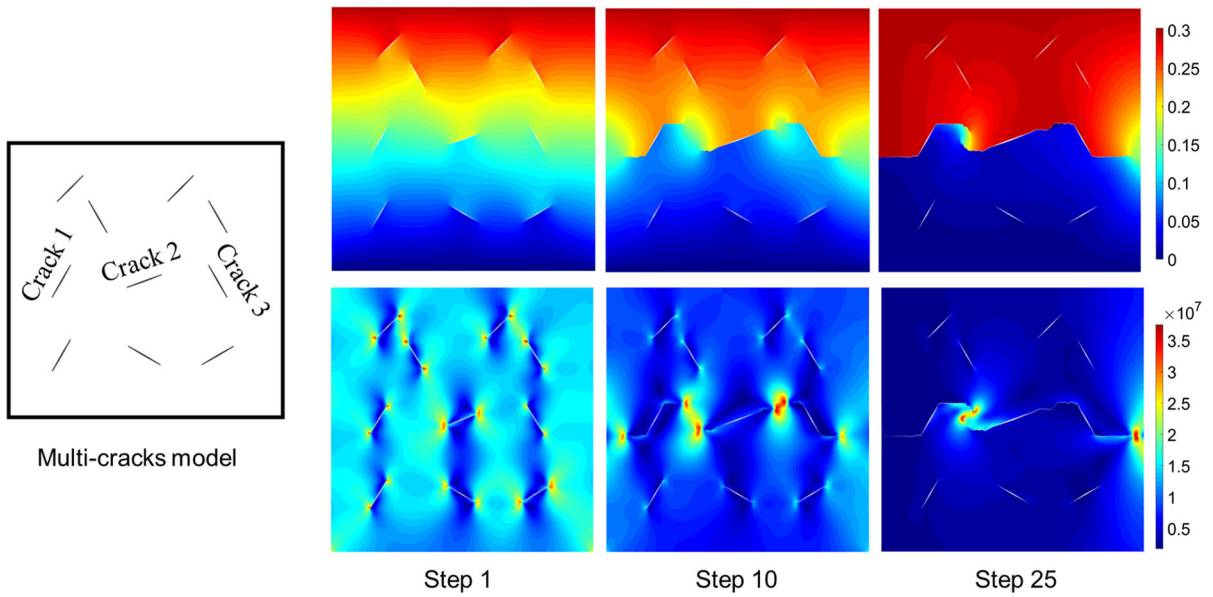
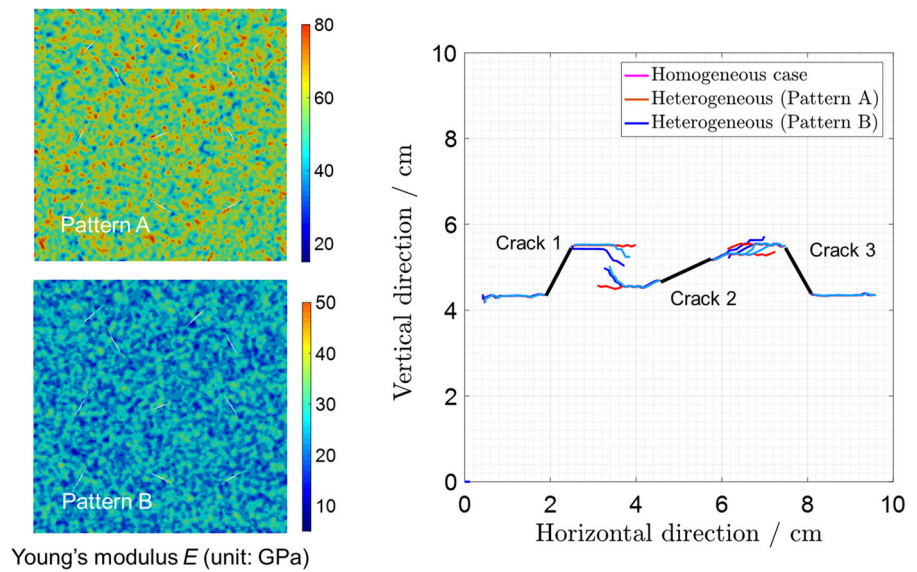


Fig. 26 Crack trajectories in a homogeneous medium with multi-crack. The displacement (unit: cm) and von Mises stress (unit: Pa). The animation of crack growth is accessible in Supplementary Data

Fig. 27 Comparison of crack trajectories in homogeneous and heterogeneous media of multi-crack growth



this context the cracks eventually coalesce in one large crack.

Furthermore, as displayed in Fig. 28, a line is placed crossing the three propagated cracks, to further explore the effect of material heterogeneity on stress analysis. It appears that the heterogeneity induces some fluctuations in both the stress and displacement fields. These fluctuations are random and may change the local distribution of stress around the crack tips. Therefore,

the SIFs evaluated at crack tips (A, B, C and D) in homogeneous and heterogeneous media are different, as depicted in Fig. 29a, where the SIFs K_I and K_{II} are represented by the normalized SIF ratio defined by $\bar{K} = (2/\pi) \arctan(K_I/K_{II})$. It implies that the cracks tend to mode-I (tensile failure) if $\bar{K} > 0.5$ and tend to mode-II (shear failure) if $\bar{K} < 0.5$. The dominance of K_I and K_{II} is the same when $\bar{K} = 0.5$. The effect of K_I on the tips B and C is relatively larger than on

Fig. 28 Distributions of **a** von Mises stress and **b** displacement when stress state satisfies propagation criterion of multi-crack growth

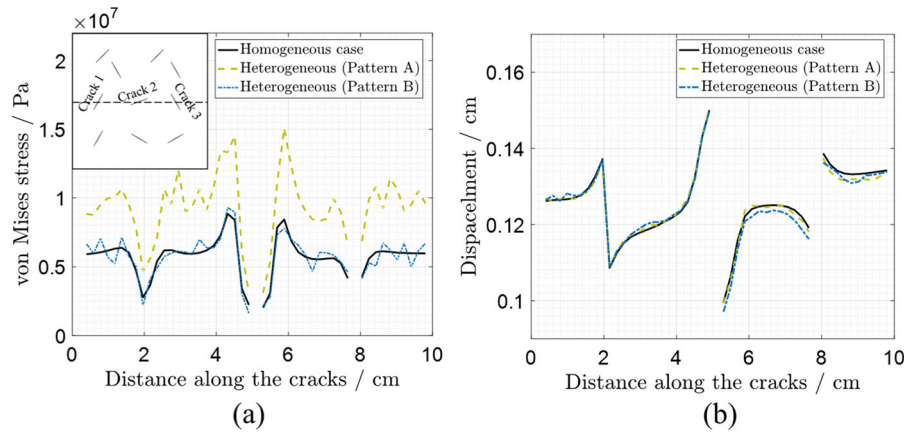
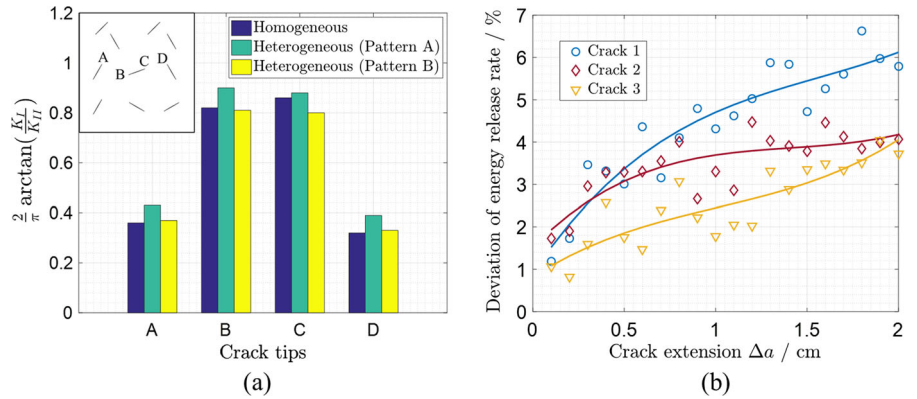


Fig. 29 **a** The normalized SIF ratio evaluated at different crack tips and **b** the influence of heterogeneity on energy release rate compared to homogeneity



the tips A and D. Figure 29b shows the influence of heterogeneity on energy release rate. To achieve this, we calculated the deviation of energy release rate in heterogeneous material compared to that in homogeneous material. The results indicate that the deviations in the crack growth process are randomly distributed, but the overall trend is an increase. The heterogeneity either amplify or diminish the SIFs, contingent on the collaborative effect of the heterogeneity and crack interaction.

5 Conclusions and implications

In this work, an improved singular-FEM has been developed for simulating multi-crack growth in heterogeneous fractured media. Then, the influences of crack interaction, loading condition and material heterogeneity on crack trajectory, crack tip field and energy release rate were clarified.

The highlights of the proposed method are summarized as follows:

- (1) This method is able to integrate the effect of heterogeneity and straightforwardly model multi-crack growth, with an efficient algorithm for simulating crack propagation and interaction.
- (2) A novel five-node singular triangular element is used to reproduce the stress singularity in the vicinity of crack tips.
- (3) The region far away from the tips can be discretized by the linear triangular elements instead of the quadratic or transition elements in the traditional FEM.

The main concluding remarks and implications are summarized as follows:

- (1) The method was applied to complicated cases with material heterogeneity and multi-crack growth. Numerical performance was examined by a benchmark study. The results prove that the improved singular-FEM is more accurate than those of FEM (LTE) and almost as accurate as FEM (QPE). It provides a compromise strategy that combining the merits of low cost and high accuracy. It also illus-

trates that material heterogeneity has a slight influence on convergence performance as well as the variation of strain energy.

- (2) Numerical results demonstrate that the initial length of crack has obvious effect on energy release rate and SIFs, which depend on the collaboration of heterogeneity and crack interaction. On the one hand, the heterogeneity may improve or reduce material strength. On the other hand, the distance between two cracks has strong effect on the variation of energy release rate. The closer the distance, the more energy is released.
- (3) The mechanism behind multi-crack growth in heterogeneous material is complicated due to the combined mechanism of heterogeneity and crack interaction. Although the crack trajectory depends on the finite element grids, this impact will be eliminated once the resolution reaches a specified value. During crack propagation, the deviation of the energy release rate of the heterogeneous material from that of the homogeneous material is distributed randomly, but the overall trend is increasing.

Acknowledgements This research was financially supported by the Research Grants Council (RGC) of Hong Kong Special Administrative Region Government (HKSARG) of China (Grant No.: R5037-18F).

Author contributions Luyu WANG: Conceptualization, Methodology, Software, Validation, Formal analysis, Writing - original draft. Zhen-Yu YIN: Formal analysis, Project administration, Funding acquisition, Supervision, Writing - review & editing. Weizhong CHEN: Formal analysis, Supervision, Writing - review & editing.

Funding Open access funding provided by The Hong Kong Polytechnic University

Declarations

Competing interests The authors declare that they have no known competing financial interests or personal relationships that could have appeared to influence the work reported in this paper.

Open Access This article is licensed under a Creative Commons Attribution 4.0 International License, which permits use, sharing, adaptation, distribution and reproduction in any medium or format, as long as you give appropriate credit to the original author(s) and the source, provide a link to the Creative Commons licence, and indicate if changes were made. The images or other third party material in this article are included in the article's Creative Commons licence, unless indicated otherwise in a credit line to the material. If material is not included in the article's Cre-

ative Commons licence and your intended use is not permitted by statutory regulation or exceeds the permitted use, you will need to obtain permission directly from the copyright holder. To view a copy of this licence, visit <http://creativecommons.org/licenses/by/4.0/>.

References

- Al-Ostaz A, Jasiuk I (1997) Crack initiation and propagation in materials with randomly distributed holes. *Eng Frac Mech* 58(5–6):395–420. [https://doi.org/10.1016/S0013-7944\(97\)00039-8](https://doi.org/10.1016/S0013-7944(97)00039-8)
- Alzabedeh K, Al-Ostaz A, Jasiuk I, Ostoja-Starzewski M (1998) Fracture of random matrix-inclusion composites: scale effects and statistics. *Int J Solids Struct* 35(19):2537–2566. [https://doi.org/10.1016/S0020-7683\(97\)00143-1](https://doi.org/10.1016/S0020-7683(97)00143-1)
- Atkinson C, Smelser RE, Sanchez J (1982) Combined mode fracture via the cracked Brazilian disk test. *Int J Frac* 18(4):279–291. <https://doi.org/10.1007/BF00015688>
- Azadi H, Khoei AK (2011) Numerical simulation of multiple crack growth in brittle materials with adaptive remeshing. *Int J Numer Methods Eng* 85:1017–1048. <https://doi.org/10.1002/nme.3002>
- Azócar D, Elgueta M, Rivara MC (2010) Automatic LEFM crack propagation method based on local Lepp-Delaunay mesh refinement. *Adv Eng Softw* 41:111–119. <https://doi.org/10.1016/j.advengsoft.2009.10.004>
- Barsoum RS (1976) On the use of isoparametric finite elements in linear fracture mechanics. *Int J Numer Methods Eng* 10:25–37. <https://doi.org/10.1002/nme.1620100103>
- Bathe KJ (2006) *Finite element procedures*. Prentice Hall Pearson Education Inc, Hoboken
- Bouchard PO, Bay F, Chastel Y, Toveni I (2000) Crack propagation modelling using an advanced remeshing technique. *Comput Methods Appl Mech Eng* 189:723–742. [https://doi.org/10.1016/S0045-7825\(99\)00324-2](https://doi.org/10.1016/S0045-7825(99)00324-2)
- Budyn É, Zi G, Moës N, Belytschko T (2004) A method for multiple crack growth in brittle materials without remeshing. *Int J Numer Methods Eng* 61:1741–1770. <https://doi.org/10.1002/nme.1130>
- Chan SK, Tuba IS, Wilson WK (1970) On the finite element method in linear fracture mechanics. *Eng Fract Mech* 2(1):1–17. [https://doi.org/10.1016/0013-7944\(70\)90026-3](https://doi.org/10.1016/0013-7944(70)90026-3)
- Dang-Trung H, Keilegavlen E, Berre I (2020) Numerical modeling of wing crack propagation accounting for fracture contact mechanics. *Int J Solids Struct* 204–205:233–247. <https://doi.org/10.1016/j.ijsolstr.2020.08.017>
- de Borst R (2022) Fracture and damage in quasi-brittle materials: a comparison of approaches. *Theor Appl Fract Mech* 122:103652. <https://doi.org/10.1016/j.tafmec.2022.103652>
- Erdogan F, Tuncel O, Paris PC (1962) An experimental investigation of the crack tip stress intensity factors in plates under cylindrical bending. *J Basic Eng* 84(4):542–546. <https://doi.org/10.1115/1.3658704>
- Erdogan F, Sih GC (1963) On the crack extension in plates under plane loading and transverse shear. *J Basic Eng* 85(4):519–525. <https://doi.org/10.1115/1.3656897>

- Griffith A (1921) The phenomena of rupture and flow in solids. *Philos Trans R Soc* 221:163–198
- Guinea GV, Planas J, Elices M (2000) KI evaluation by the displacement extrapolation technique. *Eng Fract Mech* 66(3):243–255. [https://doi.org/10.1016/S0013-7944\(00\)00016-3](https://doi.org/10.1016/S0013-7944(00)00016-3)
- Haeri H, Shahriar K, Marji MF, Moarefvand P (2014) Experimental and numerical study of crack propagation and coalescence in pre-cracked rock-like disks. *Int J Rock Mech Min Sci* 67:20–28. <https://doi.org/10.1016/j.ijrmms.2014.01.008>
- Henshell RD, Shaw KG (1975) Crack tip finite elements are unnecessary. *Int J Numer Methods Eng* 9:495–507. <https://doi.org/10.1002/nme.1620090302>
- Irwin GR (1957) Analysis of stresses and strains near the end of a crack traversing a plate. *J Appl Mech* 24(3):361–364. <https://doi.org/10.1115/1.4011547>
- Irwin GR (1968) Linear fracture mechanics, fracture transition, and fracture control. *Eng Fract Mech* 1(2):241–257. [https://doi.org/10.1016/0013-7944\(68\)90001-5](https://doi.org/10.1016/0013-7944(68)90001-5)
- Kakouris EG, Triantafyllou SP (2017) Phase-field material point method for brittle fracture. *Int J Numer Methods Eng* 112:1750–1776. <https://doi.org/10.1002/nme.5580>
- Kanninen MF, McEvily AJ, Popelar CH (1986) *Advanced fracture mechanics*. Oxford University Press, Oxford
- Kuang JH, Chen LS (1993) A displacement extrapolation method for two-dimensional mixed-mode crack problems. *Eng Fract Mech* 46(5):735–741. [https://doi.org/10.1016/0013-7944\(93\)90123-A](https://doi.org/10.1016/0013-7944(93)90123-A)
- Liu GR, Chen L, Nguyen-Thoi T, Zeng KY, Zhang GY (2010) A novel singular node-based smoothed finite element method (NS-FEM) for upper bound solutions of fracture problems. *Int J Numer Methods Eng* 83:1466–1497. <https://doi.org/10.1002/nme.2868>
- Miehe C, Welschinger F, Hofacker M (2010) Thermodynamically consistent phase-field models of fracture: variational principles and multi-field FE implementations. *Int J Numer Methods Eng* 83(10):1273–1311. <https://doi.org/10.1002/nme.2861>
- Mohmadsalehi M, Soghrati S (2022) An automated mesh generation algorithm for simulating complex crack growth problems. *Comput Methods Appl Mech Eng* 398:115015. <https://doi.org/10.1016/j.cma.2022.115015>
- Moran B, Shih CF (1987) A general treatment of crack tip contour integrals. *Eng Fract Mech* 35:295–310. <https://doi.org/10.1007/BF00276359>
- Mowbray DF (1970) A note on the finite element method in linear fracture mechanics. *Eng Fract Mech* 2(2):173–176. [https://doi.org/10.1016/0013-7944\(70\)90022-6](https://doi.org/10.1016/0013-7944(70)90022-6)
- Nguyen-Xuan H, Liu P, Bordas S, Natarajan S, Rabczuk T (2013) An adaptive singular ES-FEM for mechanics problems with singular field of arbitrary order. *Comput Methods Appl Mech Eng* 253:252–273. <https://doi.org/10.1016/j.cma.2012.07.017>
- Paluszny A, Matthäi SK (2009) Numerical modeling of discrete multi-crack growth applied to pattern formation in geological brittle media. *Int J Solids Struct* 46:3383–3397. <https://doi.org/10.1016/j.jisols.2009.05.007>
- Paris P, Erdogan F (1963) A critical analysis of crack propagation laws. *J Fluids Eng Trans* 85(4):528–533. <https://doi.org/10.1115/1.3656900>
- Rao BN, Rahman S (2000) An efficient meshless method for fracture analysis of cracks. *Comput Mech* 26:398–408. <https://doi.org/10.1007/s004660000189>
- Renshaw CE, Pollard DD (1994) Numerical simulation of fracture set formation: a fracture mechanics model consistent with experimental observations. *J Geophys Res* 99:9359–9372. <https://doi.org/10.1029/94JB00139>
- Romanowicz M (2022) Numerical assessment of the apparent fracture process zone length in wood under mode I condition using cohesive elements. *Theor Appl Fract Mech* 118:103229. <https://doi.org/10.1016/j.tafmec.2021.103229>
- Schöller L, Schneider D, Herrmann C, Prahs A, Nestler B (2022) Phase-field modeling of crack propagation in heterogeneous materials with multiple crack order parameters. *Comput Methods Appl Mech Eng* 395:114965. <https://doi.org/10.1016/j.cma.2022.114965>
- Sedmak A (2018) Computational fracture mechanics: an overview from early efforts to recent achievements. *Fatigue Fract Eng Mater Struct* 41:2438–2474. <https://doi.org/10.1111/ffe.12912>
- Shewchuk JR (2002) Delaunay refinement algorithms for triangular mesh generation. *Comput Geom Theory Appl* 22:21–74. [https://doi.org/10.1016/S0925-7721\(01\)00047-5](https://doi.org/10.1016/S0925-7721(01)00047-5)
- Sih GC (1991) *Mechanics of fracture initiation and propagation*. Springer, Dordrecht
- Silling SA, Weckner O, Askari E, Bobaru F (2010) Crack nucleation in a peridynamic solid. *Int J Frac* 162:219–227. <https://doi.org/10.1007/s10704-010-9447-z>
- Smith M (2009) ABAQUS/Standard User's Manual Version 6.9. Dassault Systèmes Simulia Corp
- Tan X, Chen W, Wang L, Yang J, Tan X (2021) Settlement behaviors investigation for underwater tunnel considering the impacts of fractured medium and water pressure. *Mar Georesources Geotechnol* 39:639–648. <https://doi.org/10.1080/1064119X.2020.1737279>
- Tracey DM (1970) Finite elements for determination of crack tip elastic stress intensity factors. *Eng Fract Mech* 3(3):255–265. [https://doi.org/10.1016/0013-7944\(71\)90036-1](https://doi.org/10.1016/0013-7944(71)90036-1)
- Ucar E, Keilegavlen E, Berre I, Nordbotten JM (2018) A finite-volume discretization for deformation of fractured media. *Comput Geosci* 22:993–1007. <https://doi.org/10.1007/s10596-018-9734-8>
- Wang L, Chen W, Tan X, Yang J (2019) The impact of various crack geometrical parameters on stress field over tip under different mixed loading conditions and inclination angles. *Theor Appl Fract Mech* 102:239–254. <https://doi.org/10.1016/j.tafmec.2018.12.001>
- Wang L, Chen W, Tan X, Yang Tan XJ., Yang D, Zhang X (2020) Numerical investigation on the stability of deforming fractured rocks using discrete fracture networks: a case study of underground excavation. *Bull Eng Geol Environ* 79:133–151. <https://doi.org/10.1007/s10064-019-01536-9>
- Wang M, Gao K, Feng YT (2021) An improved continuum-based finite-discrete element method with intra-element fracturing algorithm. *Comput Methods Appl Mech Eng* 384:113978. <https://doi.org/10.1016/j.cma.2021.113978>
- Wang L, Vuik C, Hajibeygi H (2022a) A stabilized mixed-FE scheme for frictional contact and shear failure analyses in deformable fractured media. *Eng Fract Mech* 267:108427. <https://doi.org/10.1016/j.engfractmech.2022.108427>

- Wang L, Chen W, Vuik C (2022b) Hybrid-dimensional modeling for fluid flow in heterogeneous porous media using dual fracture-pore model with flux interaction of fracture-cavity network. *J Nat Gas Sci Eng* 100:104450. <https://doi.org/10.1016/j.jngse.2022.104450>
- Wang L, Chen W, Zhang Y, Zhang X, Vuik C (2022c) Investigating effects of heterogeneity and fracture distribution on two-phase flow in fractured reservoir with adaptive time strategy. *Transp Porou Media*. <https://doi.org/10.1007/s11242-022-01850-z>
- Weißgraber P, Leguillon D, Becker W (2016) A review of Finite Fracture Mechanics: crack initiation at singular and non-singular stress raisers. *Arch Appl Mech* 86:375–401. <https://doi.org/10.1007/s00419-015-1091-7>
- Yukio U, Kazuo I, Tetsuya Y, Mitsuru A (1983) Characteristics of brittle fracture under general combined modes including those under bi-axial tensile loads. *Eng Fract Mech* 18(6):1131–1158. [https://doi.org/10.1016/0013-7944\(83\)90007-3](https://doi.org/10.1016/0013-7944(83)90007-3)
- Zehnder AT (2012) *Fracture mechanics*. Springer, Berlin
- Zhang P, Du C, Birk C, Zhao W (2019) A scaled boundary finite element method for modelling wing crack propagation problems. *Eng Fract Mech* 216:106466. <https://doi.org/10.1016/j.engfracmech.2019.04.040>
- Zhang Y, Zou Y, Zhang Y, Wang L, Liu D, Sun J, Ge H, Zhou D (2022) Experimental study on characteristics and mechanisms of matrix pressure transmission near the fracture surface during post-fracturing shut-in in tight oil reservoirs. *J Pet Sci Eng* 291:111133. <https://doi.org/10.1016/j.petrol.2022.111133>
- Zienkiewicz OC, Taylor LR (2000) *The finite element method: solid mechanics*. Butterworth-Heinemann, Oxford

Publisher's Note Springer Nature remains neutral with regard to jurisdictional claims in published maps and institutional affiliations.